ORIGINAL PAPER

Size-effects of metamaterial beams subjected to pure bending: on boundary conditions and parameter identification in the relaxed micromorphic model

Mohammad Sarhil[1] · Lisa Scheunemann[2] · Jörg Schröder[1] · Patrizio Neff[3]

Abstract

In this paper we model the size-effects of metamaterial beams under bending with the aid of the relaxed micromorphic continuum. We analyze first the size-dependent bending stiffness of heterogeneous fully discretized metamaterial beams subjected to pure bending loads. Two equivalent loading schemes are introduced which lead to a constant moment along the beam length with no shear force. The relaxed micromorphic model is employed then to retrieve the size-effects. We present a procedure for the determination of the material parameters of the relaxed micromorphic model based on the fact that the model operates between two well-defined scales. These scales are given by linear elasticity with micro and macro elasticity tensors which bound the relaxed micromorphic continuum from above and below, respectively. The micro elasticity tensor is specified as the maximum possible stiffness that is exhibited by the assumed metamaterial while the macro elasticity tensor is given by standard periodic first-order homogenization. For the identification of the micro elasticity tensor, two different approaches are shown which rely on affine and non-affine Dirichlet boundary conditions of candidate unit cell variants with the possible stiffest response. The consistent coupling condition is shown to allow the model to act on the whole intended range between macro and micro elasticity tensors for both loading cases. We fit the relaxed micromorphic model against the fully resolved metamaterial solution by controlling the curvature magnitude after linking it with the specimen's size. The obtained parameters of the relaxed micromorphic model are tested for two additional loading scenarios.

Keywords Size-effects · Consistent coupling condition · Metamaterials · Relaxed micromorphic model · Generalized continua · Homogenization

1 Introduction

Mechanical metamaterials are unconventional materials with exotic mechanical properties that are governed by the geometry of the complex underlying microstructure rather than by the properties of the constituting materials [34, 44, 62, 122, 124]. They can be optimized to obtain the intended mechanical properties to fit the wanted functionality [111]. However,

mechanical metamaterials typically reveal size-effect phenomena and therefore the classical Cauchy–Boltzmann theory and first-order homogenization methods are incapable to describe such mechanical behavior. Generalized continua are enhanced continua that can model these size-effects as a homogeneous continuum without accounting for the detailed microstructure. The enhancement can be achieved by expanding the kinematics to contain additional degrees of freedom, e.g. the classical micromorphic theory [31, 32, 49, 71, 77, 110] and the Cosserat theory [9, 24, 63, 76, 78, 114], or by accounting for higher-grade differential operators in the energy functional, e.g. gradient elasticity models [5, 11–13, 30, 33, 43, 72, 102, 119]. However, the identification of the material parameters of these models is not trivial and in general remains unsolved. Different schemes were presented for the homogenization of the heterogeneous fully resolved microstructures into the Cosserat continuum in [9, 37, 47, 84], different variants of the gradient elasticity continuum

✉ Mohammad Sarhil
mohammad.sarhil@uni-due.de

1 Institute of Mechanics, University of Duisburg-Essen,
Universitätsstr. 15, 45141 Essen, Germany

2 Chair of Applied Mechanics, RPTU Kaiserslautern-Landau,
Gottlieb-Daimler-Str., 67663 Kaiserslautern, Germany

3 Chair of Nonlinear Analysis and Modeling, Faculty of
Mathematics, University of Duisburg-Essen,
Thea-Leymann-Str. 9, 45141 Essen, Germany

in [2, 3, 16, 51, 60, 99, 104, 116–118, 120] and the classical Eringen–Mindlin micromorphic continuum in [8, 20, 35, 46, 93–95, 125], however, without leading to a universally accepted answer. Mainly two approaches are employed for the determination of higher-order homogenized properties, which are asymptotic expansion methods, see e. g. [15, 22] (also in combination with fast Fourier transform methods, see [65, 112]) and heuristic approaches relying upon the ad-hoc definition of modified kinematic boundary conditions on the microscale compared to first-order problems, see [19, 43]. Among the latter, quadratic boundary conditions have been applied and analyzed to a large extent, see e. g. [14, 35, 36, 38, 58, 59, 113], in the field of homogenization towards second gradient continua and classical micromorphic continua. However, several problematic issues are described in the literature for this choice. Indeed, this natural extension does not lead to vanishing effective higher-order moduli when a homogeneous RVE or unit cell is homogenized. Moreover, when scale separation holds, Cauchy theory is also not a priori recovered, cf. [8]. To correct some of these spurious effects, additional microstructure-dependent body forces along with quadratic boundary conditions have been introduced [73, 123]. Even though the presented results agree well with results from asymptotic homogenization, there remain artifacts for the special case of soft inclusions in a hard matrix material, for which the higher-order properties diverge. An alternative formulation has been proposed in [47] by averaging solely over microheterogeneities in a homogenization scheme from a Cauchy continuum to micromorphic media. Note that [113] stated that a quartic boundary condition would be necessary for fully describing the moduli in a micromorphic theory. A harmonic decomposition is recently applied to the governing equations and used to interpret the related modes on the micro-scale in [48]. A variational approach is presented for the homogenization from a Cauchy continuum on the lower scale towards a second gradient or micromorphic continuum on the macro-scale in [8, 39], respectively. In their approach, as in other theories, the microscopic displacement is decomposed into a homogeneous and a fluctuation part. However, in contrast to other theories involving a heuristic definition of boundary conditions, the homogeneous part of the deformation arises here from a variational approach.

With an enhancement of the description on the microlevel [116] presents a homogenization procedure from metamaterial unit cell structures modeled using beam-lattice structures on the micro-scale to a second gradient linear elastic model on the macro-scale. Similar to [38], zero energy modes are observed for the higher-order moduli. In [99], a homogenization strategy for higher-order continua is presented which scales from a second-order continuum on the meso-scale to second- and third-order continua on the macro-scale under application of Isogeometric Analysis (IGA) and thereby also

enhances the micro-scale continuum. Further developments in the context of multiphysical applications are e.g. discussed in [115].

In the field of asymptotic expansion homogenization and especially homogenization of metamaterials, the authors in [4] have used asymptotic homogenization for the analysis of different unit cells in the framework of metamaterials. They exploited insight on the beam bending problem with a focus on the observable size-effects. In [2], metamaterials with honeycomb microstructure are analyzed in the framework of asymptotic expansion homogenization. The work [3] presents a straight forward computational scheme for the determination of effective moduli through comparison with microstructure simulations. Here, the model is chosen apriori and does not originate from a homogenization strategy.

Numerical and analytical solutions have been compared on a 3D structure for different deformation modes in [119] and pointed out the necessity of wedge and double traction forces for a correct overlap of both solutions. In [117], mechanical metamaterials are analyzed by means of asymptotic expansion with an eye on appearing size-effects, which could only be detected for shear and torsion modes.

The relaxed micromorphic model considered by us is a generalized continuum model that allows in principle to capture size-effects and to describe band gaps phenomena in the dynamical case, see for example [6, 18, 25, 28, 67–70, 88, 90, 90, 91]. This model has been introduced in [40, 79] and its well-posedness for the static and dynamic problems has been proved in [80, 82]. In [55] the regularity of the model was investigated. Being a micromorphic model, it features the classical translational degrees of freedom $\boldsymbol{u} : \mathcal{B} \in \mathbb{R}^3 \to \mathbb{R}^3$ as well as a non-symmetric micro-distortion field $\boldsymbol{P} : \mathcal{B} \in \mathbb{R}^3 \to \mathbb{R}^{3\times3}$. Compared to the classical micromorphic approach, the assumed strain energy is drastically simplified; notably, the curvature part (derivatives of $\boldsymbol{P}$) intervenes only through $\mathrm{Curl}\,\boldsymbol{P}$, so that solutions are found in $H^1(\mathcal{B}) \times H(\mathrm{curl}, \mathcal{B})$ for the pair $(\boldsymbol{u}, \boldsymbol{P})$. Using only the Curl of $\boldsymbol{P}$ has some decisive advantages. It generates "bounded stiffness" [85–87, 89] for arbitrary large characteristic length (arbitrary small samples), in opposition to all strain gradient, Cosserat-micropolar or classical micromorphic approaches. Moreover, the appearing length-scale independent elasticity tensors $\mathbb{C}_e$ and $\mathbb{C}_{\mathrm{micro}}$ are related by a Reuss-like homogenization formula as function of the uniquely known elasticity tensor $\mathbb{C}_{\mathrm{macro}}$ from classical periodic homogenization. It remains therefore to determine $\mathbb{C}_{\mathrm{micro}}$, which happens to be the largest observable stiffness in the model (such an identification does not exist for the classical micromorphic model or other variants of it). As it turns out, the relaxed micromorphic model interpolates between two well-defined scales: the classical continuum scales of macroscopic elasticity, whose stiffness is given by $\mathbb{C}_{\mathrm{macro}}$ and a microscopic scale, with stiffness $\mathbb{C}_{\mathrm{micro}}$. The role of the characteristic length $L_c > 0$

is then to scale correctly with the size of the specimen and to describe the interaction between the two scales. For $L_c \to 0$ we recover macroscopic elasticity (complete scale separation, stiffness $\mathbb{C}_{\text{macro}}$) and for $L_c \to \infty$ (zoom into the microstructure) we obtain the microscopic scale (stiffness $\mathbb{C}_{\text{micro}}$).

In this contribution, we want to explore the possibilities that this unique interpretation of the relaxed micromorphic model provides. We consider an architected material (hard matrix with soft inclusions). The determination of $\mathbb{C}_{\text{macro}}$ is a standard identification in periodic homogenization theory. The identification of $\mathbb{C}_{\text{micro}}$ will be guided by the largest stiffness idea alluded to above. Therefore, we consider a bending test of slender metamaterial beams. The size-dependent bending was analyzed by means of other enriched models such as strain gradient, Cosserat-micropolar and other continua in [4, 7, 45, 50–52, 61, 64, 66, 121]. Modeling the mechanical behavior of many metamaterials was achieved for a variety of applications using generalized continua in [1, 23, 27, 29, 42, 83, 96, 101, 103, 108, 109].

In this work the size-effects of metamaterial beams with fully discretized microstructure are analyzed. Afterward, we employ the relaxed micromorphic continuum to describe these size-effects without accounting for the detailed microstructure. The material parameters and adequate boundary conditions of the micro-distortion field $\boldsymbol{P}$ should be identified in order to establish a simplified fitting procedure on the fully resolved metamaterial beams. The so-called consistent coupling condition (applied on the Dirichlet boundary for $\boldsymbol{u}$) allows the relaxed micromorphic to operate on the whole scale between $\mathbb{C}_{\text{macro}}$ and $\mathbb{C}_{\text{micro}}$ which is of pivotal importance for a correct identification of its material parameters. However, an alternative loading by a normal linear traction (applied moment), which delivers exactly the same results for the fully resolved metamaterial, achieves consistent results as well for the relaxed micromorphic model when the consistent coupling condition is imposed via the penalty approach on the part of the boundary where the traction is set.

In a previous attempt [81] $\mathbb{C}_{\text{micro}}$ was supposed to be given by the Löwner matrix supremum $\mathbb{C}_{\text{micro}}^{L\ddot{o}wner}$ of elasticity tensors appearing under affine Dirichlet conditions on the unit cell level. From the results in the present paper it inspires that $\mathbb{C}_{\text{micro}}^{L\ddot{o}wner}$ is too soft, when compared with the appearing stiffness in the bending regime. Here, we extend our understanding of $\mathbb{C}_{\text{micro}}$ towards all scenarios, notably including non-affine Dirichlet conditions. We limit our consideration to the planar case, in which the isotropic curvature energy in terms of Curl $\boldsymbol{P}$ has only one free parameter.

The outline of the paper is as follows: in Sect. 2.1 we recall the energy functional of the relaxed micromorphic model, define the material parameters, and introduce the strong forms with the associated boundary conditions

obtained by the energy minimization. We present briefly in Sect. 2.2 the main aspects of the construction of $H(\text{curl}, \mathcal{B})$-conforming finite elements. The size-effects of the heterogeneous microstructured metamaterial beams are investigated in Sect. 3 for two loading cases which lead to the same results. In Sect. 4 we determine the material parameters of the relaxed micromorphic model and discuss the boundary condition for symmetric and non-symmetric force stresses. We then fit the relaxed micromorphic model solution to the microstructured metamaterial solution by calibrating the curvature in Sect. 5. In Sect. 6, the relaxed micromorphic model is shown to be capable of handling two loading scenarios in addition to pure bending. Finally, we provide our conclusions and outlook in Sect. 7.

2 The relaxed micromorphic model and its discretization

2.1 The relaxed micromorphic model

The relaxed micromorphic model (RMM) is an enriched continuum model. The kinematics of each material point is determined, similar to the general micromorphic theory [32, 71, 110], by a displacement vector $\boldsymbol{u} \colon \mathcal{B} \subseteq \mathbb{R}^3 \to \mathbb{R}^3$ and a non-symmetric micro-distortion field $\boldsymbol{P} \colon \mathcal{B} \subseteq \mathbb{R}^3 \to \mathbb{R}^{3 \times 3}$. The displacement and the micro-distortion fields are defined for the static case by minimizing the energy functional

$$\Pi(\boldsymbol{u}, \boldsymbol{P}) = \int_{\mathcal{B}} W(\nabla \boldsymbol{u}, \boldsymbol{P}, \text{Curl}\, \boldsymbol{P}) - \overline{\boldsymbol{f}} \cdot \boldsymbol{u} \, \mathrm{d}V$$
$$- \int_{\partial \mathcal{B}_t} \overline{\boldsymbol{t}} \cdot \boldsymbol{u} \, \mathrm{d}A \longrightarrow \text{min}, \tag{1}$$

with $(\boldsymbol{u}, \boldsymbol{P}) \in H^1(\mathcal{B}) \times H(\text{curl}, \mathcal{B})$. The vector $\overline{\boldsymbol{f}}$ describes the applied body force. The vector $\overline{\boldsymbol{t}}$ is the traction vector acting on the boundary $\partial \mathcal{B}_t \subset \partial \mathcal{B}$. The elastic energy density W reads

$$\begin{aligned} W(\nabla \boldsymbol{u}, \boldsymbol{P}, \text{Curl}\, \boldsymbol{P}) = \frac{1}{2} (\text{sym}[\nabla \boldsymbol{u} - \boldsymbol{P}] : \mathbb{C}_{\text{e}} : \text{sym}[\nabla \boldsymbol{u} - \boldsymbol{P}] \\ + \text{sym}\, \boldsymbol{P} : \mathbb{C}_{\text{micro}} : \text{sym}\, \boldsymbol{P} \\ + \text{skew}[\nabla \boldsymbol{u} - \boldsymbol{P}] : \mathbb{C}_{\text{c}} : \text{skew}[\nabla \boldsymbol{u} - \boldsymbol{P}] \\ + \mu L_{\text{c}}^2 \text{Curl}\, \boldsymbol{P} : \mathbb{L} : \text{Curl}\, \boldsymbol{P}). \end{aligned} \tag{2}$$

Here, $\mathbb{C}_{\text{micro}}, \mathbb{C}_{\text{e}} > \boldsymbol{0}$ are fourth-order positive definite standard elasticity tensors, $\mathbb{C}_{\text{c}} \geq \boldsymbol{0}$ is a fourth-order positive semi-definite rotational coupling tensor, $\mathbb{L}$ is a positive definite fourth-order tensor acting on non-symmetric arguments, $L_{\text{c}} \geq 0$ is the characteristic length parameter and μ is a shear modulus for dimensional consistency. The characteristic length parameter is related to the size of the microstructure

and determines its influence on the macroscopic mechanical behavior. The characteristic length allows to scale the number of considered unit cells keeping all remaining parameters of the model scale-independent where the macro-scale with $\mathbb{C}_{\text{macro}}$ and the micro-scale with $\mathbb{C}_{\text{micro}}$ are retrieved for $L_{\text{c}} \to 0$ and $L_{\text{c}} \to \infty$, respectively, if suitable boundary conditions are applied, see [81, 100]. The macro-scale elasticity tensor $\mathbb{C}_{\text{macro}}$ associated with $L_{\text{c}} \to 0$ can be defined by the standard first-order periodic homogenization (the scale separation holds) while the micro-scale elasticity tensor $\mathbb{C}_{\text{micro}}$ associated with $L_{\text{c}} \to \infty$ represents the stiffest extrapolated response (zooming in the microstructure). The constitutive coefficients are assumed constant with the following symmetries

$$
\begin{aligned}
&(\mathbb{C}_{\text{micro}})_{ijkl} = (\mathbb{C}_{\text{micro}})_{klij} = (\mathbb{C}_{\text{micro}})_{jikl}, \\
&(\mathbb{C}_{\text{c}})_{ijkl} = (\mathbb{C}_{\text{c}})_{klij}, \\
&(\mathbb{C}_{\text{e}})_{ijkl} = (\mathbb{C}_{\text{e}})_{klij} = (\mathbb{C}_{\text{e}})_{jikl}, \\
&(\mathbb{L})_{ijkl} = (\mathbb{L})_{klij},
\end{aligned}
\tag{3}
$$

where $\mathbb{C}_{\text{micro}}$ and $\mathbb{C}_{\text{e}}$ are connected to $\mathbb{C}_{\text{macro}}$ through a Reuss-like homogenization relation [17]

$$
\begin{aligned}
&\mathbb{C}_{\text{macro}}^{-1} = \mathbb{C}_{\text{micro}}^{-1} + \mathbb{C}_{\text{e}}^{-1} \\
&\Rightarrow \quad \mathbb{C}_{\text{e}} = \mathbb{C}_{\text{micro}}(\mathbb{C}_{\text{micro}} - \mathbb{C}_{\text{macro}})^{-1}\mathbb{C}_{\text{macro}}.
\end{aligned}
\tag{4}
$$

The variation of the potential with respect to the displacement yields the weak form

$$
\begin{aligned}
\delta_{\boldsymbol{u}}\Pi = \int_{\mathcal{B}} \{\underbrace{\mathbb{C}_{\text{e}} : \text{sym}[\nabla\boldsymbol{u} - \boldsymbol{P}] + \mathbb{C}_{\text{c}} : \text{skew}[\nabla\boldsymbol{u} - \boldsymbol{P}]\}}_{=:\,\boldsymbol{\sigma}} : \nabla\delta\boldsymbol{u} \\
- \bar{\boldsymbol{f}} \cdot \delta\boldsymbol{u} \, dV - \int_{\partial\mathcal{B}_t} \bar{\boldsymbol{t}} \cdot \delta\boldsymbol{u} \, dA = 0,
\end{aligned}
\tag{5}
$$

which leads, using integration by parts and employing the divergence theorem, to

$$
\delta_{\boldsymbol{u}}\Pi = \int_{\mathcal{B}} \{\text{div } \boldsymbol{\sigma} + \bar{\boldsymbol{f}}\} \cdot \delta\boldsymbol{u} \, dV = 0,
\tag{6}
$$

where $\boldsymbol{\sigma}$ is the non-symmetric force stress tensor (symmetric if $\mathbb{C}_{\text{c}} \equiv \boldsymbol{0}$ which is permitted). In a similar way, the variation of the potential with respect to the micro-distortion field $\boldsymbol{P}$ leads to the weak form

$$
\begin{aligned}
\delta_{\boldsymbol{P}}\Pi = \int_{\mathcal{B}} \{\boldsymbol{\sigma} - \underbrace{\mathbb{C}_{\text{micro}} : \text{sym}\,\boldsymbol{P}}_{=:\,\boldsymbol{\sigma}_{\text{micro}}}\} : \delta\boldsymbol{P} \\
- \underbrace{\mu\, L_{\text{c}}^2(\mathbb{L} : \text{Curl}\,\boldsymbol{P})}_{=:\,\boldsymbol{m}} : \text{Curl}\,\delta\boldsymbol{P} \, dV = 0,
\end{aligned}
\tag{7}
$$

which can be rewritten, using integration by parts and applying Stokes' theorem, as

$$
\begin{aligned}
\delta_{\boldsymbol{P}}\Pi = \int_{\mathcal{B}} \{\boldsymbol{\sigma} - \boldsymbol{\sigma}_{\text{micro}} - \text{Curl}\,\boldsymbol{m}\} : \delta\boldsymbol{P} \, dV \\
+ \int_{\partial\mathcal{B}} \{\sum_{i=1}^{3}\left(\boldsymbol{m}^i \times \delta\boldsymbol{P}^i\right) \cdot \boldsymbol{n}\} \, dA = 0,
\end{aligned}
\tag{8}
$$

where the stress measurements $\boldsymbol{\sigma}_{\text{micro}}$ and $\boldsymbol{m}$ are the micro- and moment stresses, respectively, $\boldsymbol{n}$ is the outward unit normal vector on the boundary, and $\boldsymbol{m}^i$ and $\delta\boldsymbol{P}^i$ are the row vectors of the related second-order tensors. The strong form of the relaxed micromorphic model with the associated boundary conditions read

$$
\begin{aligned}
&\text{div } \boldsymbol{\sigma} + \bar{\boldsymbol{f}} = \boldsymbol{0} && \text{on} \quad \mathcal{B}, && \text{(9a)} \\
&\boldsymbol{u} = \bar{\boldsymbol{u}} && \text{on} \quad \partial\mathcal{B}_u, && \text{(9b)} \\
&\bar{\boldsymbol{t}} = \boldsymbol{\sigma} \cdot \boldsymbol{n} && \text{on} \quad \partial\mathcal{B}_t, && \text{(9c)} \\
&\boldsymbol{\sigma} - \boldsymbol{\sigma}_{\text{micro}} - \text{Curl}\,\boldsymbol{m} = 0 && \text{on} \quad \mathcal{B}, && \text{(9d)} \\
&\sum_{i=1}^{3}\boldsymbol{P}^i \times \boldsymbol{n} = \bar{\boldsymbol{t}}_P && \text{on} \quad \partial\mathcal{B}_P, && \text{(9e)} \\
&\sum_{i=1}^{3}\boldsymbol{m}^i \times \boldsymbol{n} = \boldsymbol{0} && \text{on} \quad \partial\mathcal{B}_m, && \text{(9f)}
\end{aligned}
$$

where $\partial\mathcal{B}_P \cap \partial\mathcal{B}_m = \partial\mathcal{B}_u \cap \partial\mathcal{B}_t = \emptyset$ and $\partial\mathcal{B}_P \cup \partial\mathcal{B}_m = \partial\mathcal{B}_u \cup \partial\mathcal{B}_t = \partial\mathcal{B}$. The strong form represents a generalized balance of linear momentum (force balance) and a generalized balance of angular momentum (moment balance). For more details regarding derivations of the boundary conditions, the reader is referred to [100].

An additional dependence between the displacement field and the micro-distortion field on the boundary was proposed in [81] and subsequently considered in [26, 85, 86, 105]. This so-called *consistent coupling condition* is defined by

$$
\begin{aligned}
\boldsymbol{P} \cdot \boldsymbol{\tau} = \nabla\boldsymbol{u} \cdot \boldsymbol{\tau} \Leftrightarrow \boldsymbol{P}^i \times \boldsymbol{n} = \nabla\boldsymbol{u}^i \times \boldsymbol{n} \\
\text{for} \quad i = 1, 2, 3 \quad \text{on} \quad \partial\mathcal{B}_P = \partial\mathcal{B}_u,
\end{aligned}
\tag{10}
$$

where $\boldsymbol{\tau}$ is the tangential vector on the boundary and $\boldsymbol{P}_i$ and $\nabla\boldsymbol{u}^i$ are the row-vectors of the associated tensors. However, we can extend this relative boundary condition to parts of $\partial\mathcal{B}_m$ by enforcing the consistent coupling condition on $\partial\mathcal{B}_{\widehat{m}} \subseteq \partial\mathcal{B}_m$ via a penalty approach as

$$
\Pi \Leftarrow \Pi + \int_{\partial\mathcal{B}_{\widehat{m}}} \frac{\kappa_1}{2} \sum_{i=1}^{3} ||(\boldsymbol{P}^i - \nabla\boldsymbol{u}^i) \times \boldsymbol{n})||^2 \, dA,
\tag{11}
$$

where κ_1 is the penalty parameter.

The micro-distortion field has the following general form for the three-dimensional case

$$
\boldsymbol{P} = \begin{pmatrix} (\boldsymbol{P}^1)^T \\ (\boldsymbol{P}^2)^T \\ (\boldsymbol{P}^3)^T \end{pmatrix} = \begin{pmatrix} P_{11} & P_{12} & P_{13} \\ P_{21} & P_{22} & P_{23} \\ P_{31} & P_{32} & P_{33} \end{pmatrix} \quad \text{with}
$$

$$
\boldsymbol{P}^i = \begin{pmatrix} P_{i1} \\ P_{i2} \\ P_{i3} \end{pmatrix} \text{ for } i = 1, 2, 3. \tag{12}
$$

We let the Curl operator act on the row vectors of the micro-distortion field $\boldsymbol{P}$ as

$$
\text{Curl}\,\boldsymbol{P} = \begin{pmatrix} (\text{curl}\,\boldsymbol{P}^1)^T \\ (\text{curl}\,\boldsymbol{P}^2)^T \\ (\text{curl}\,\boldsymbol{P}^3)^T \end{pmatrix}
$$

$$
= \begin{pmatrix} P_{13,2} - P_{12,3} & P_{11,3} - P_{13,1} & P_{12,1} - P_{11,2} \\ P_{23,2} - P_{22,3} & P_{21,3} - P_{23,1} & P_{22,1} - P_{21,2} \\ P_{33,2} - P_{32,3} & P_{31,3} - P_{33,1} & P_{32,1} - P_{31,2} \end{pmatrix}. \tag{13}
$$

2.2 $H^1(\mathcal{B}) \times H(\text{curl}, \mathcal{B})$-conforming finite element in 2D

Different finite element formulations of the relaxed micromorphic model were introduced for the plane strain case in [97, 98, 100], antiplane shear in [105] and 3D case in [106, 107]. For the two-dimensional case, the micro-distortion field has only four non-vanishing components, which are in the plane, and its Curl operator is reduced to only two components out of the plane, namely $(\text{Curl}\,\boldsymbol{P})_{13}$ and $(\text{Curl}\,\boldsymbol{P})_{23}$,

$$
\boldsymbol{P} = \begin{pmatrix} (\boldsymbol{P}^1)^T \\ (\boldsymbol{P}^2)^T \\ \boldsymbol{0}^T \end{pmatrix} = \begin{pmatrix} P_{11} & P_{12} & 0 \\ P_{21} & P_{22} & 0 \\ 0 & 0 & 0 \end{pmatrix} \quad \text{and}
$$

$$
\text{Curl}\,\boldsymbol{P} = \begin{pmatrix} 0 & 0 & P_{12,1} - P_{11,2} \\ 0 & 0 & P_{22,1} - P_{21,2} \\ 0 & 0 & 0 \end{pmatrix}. \tag{14}
$$

It has been shown in [100] that $H^1(\mathcal{B}) \times H(\text{curl}, \mathcal{B})$ elements obtain the discontinuous solution of the micro-distortion field while the standard nodal $H^1(\mathcal{B}) \times H^1(\mathcal{B})$ elements are unable to capture the jumps. Therefore, transition zones emerge for $H^1(\mathcal{B}) \times H^1(\mathcal{B})$ elements which need to be resolved by distinctly refining the mesh in contrast to $H^1(\mathcal{B}) \times H(\text{curl}, \mathcal{B})$ elements which exhibit faster convergences rates.

We demonstrate briefly the main aspects of the finite element formulation of a quadrilateral element $(\boldsymbol{u}, \boldsymbol{P}) \in H^1(\mathcal{B}) \times H(\text{curl}, \mathcal{B})$ shown in Fig. 1. The finite element, denoted as Q2NQ2, utilizes Lagrange-type shape functions of the second-order for the displacement field, denoted as
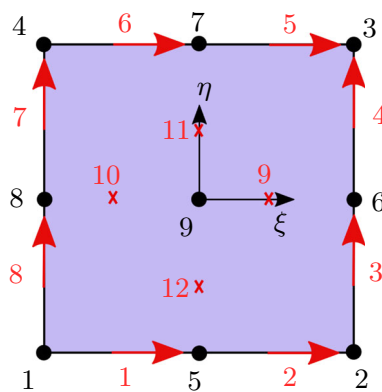

Fig. 1 Q2NQ2 element. Black dots represent the displacement nodes. Red arrows and crosses indicate the edge and inner vectorial dofs, respectively, of the micro-distortion field used in Nédélec formulation

Q2. The suitable finite element space for the micro-distortion field is known as Nédélec space, see [74, 75]. In this work, we choose the Nédélec space of first-kind and second-order, denoted as NQ2. Nédélec formulation uses vectorial shape functions that satisfy the tangential continuity at element interfaces. General reviews about the edge elements are available in [54, 92]. For more details regarding the derivation of shape functions and the FEM-implementation aspects, the reader is referred to [100].

The Q2NQ2 element uses 9 nodes for the discretization of the displacement field $\boldsymbol{u}$. The geometry and the displacement field are approximated employing the related quadratic scalar shape functions N_I^u defined in the parameter space with natural coordinates $\boldsymbol{\xi} = \{\xi, \eta\}$ by

$$
\boldsymbol{X}_h = \sum_{I=1}^{9} N_I^u(\boldsymbol{\xi})\,\boldsymbol{X}_I, \qquad \boldsymbol{u}_h = \sum_{I=1}^{9} N_I^u(\boldsymbol{\xi})\,\boldsymbol{d}_I^u, \tag{15}
$$

where $\boldsymbol{X}_I$ are the coordinates of the displacement node I and $\boldsymbol{d}_I^u$ are its displacement degrees of freedom. The deformation gradient is obtained then in physical space by

$$
\nabla \boldsymbol{u}_h = \sum_{I=1}^{9} \boldsymbol{d}_I^u \otimes \nabla N_I^u(\boldsymbol{\xi}), \quad \text{with} \quad \nabla N_I^u(\boldsymbol{\xi}) = \boldsymbol{J}^{-T} \cdot \nabla_{\boldsymbol{\xi}} N_I^u, \tag{16}
$$

where $\boldsymbol{J} = \frac{\partial \boldsymbol{X}}{\partial \boldsymbol{\xi}}$ is the Jacobian, ∇ and $\nabla_{\boldsymbol{\xi}}$ are the gradient operators to $\boldsymbol{X}$ and $\boldsymbol{\xi}$, respectively. The micro-distortion field $\boldsymbol{P}$ is approximated by the vectorial dofs $\boldsymbol{d}_I^P$ presenting its tangential components at the location $I = 1, \dots, 12$. The micro-distortion field and its Curl operator are interpolated as

$$
\boldsymbol{P}_h = \sum_{I=1}^{12} \boldsymbol{d}_I^P \otimes \boldsymbol{\psi}_I^2, \qquad \text{Curl}\,\boldsymbol{P}_h = \sum_{I=1}^{12} \boldsymbol{d}_I^P \otimes \text{curl}\,\boldsymbol{\psi}_I^2. \tag{17}
$$

The non-vanishing components of the Curl operator of the micro-distortion field for the 2D case are obtained by

$$
\begin{bmatrix} \text{curl}^{2D} \, \boldsymbol{P}_h^1 \\ \text{curl}^{2D} \, \boldsymbol{P}_h^2 \end{bmatrix} = \sum_{I=1}^{12} \boldsymbol{d}_I^P \, \text{curl}^{2D} \, \boldsymbol{\psi}_I^2 = \begin{bmatrix} \sum_{I=1}^{12} (d_I^P)_1 \, \text{curl}^{2D} \, \boldsymbol{\psi}_I^2 \\ \sum_{I=1}^{12} (d_I^P)_2 \, \text{curl}^{2D} \, \boldsymbol{\psi}_I^2 \end{bmatrix}.
\tag{18}
$$

The simulations presented in this paper are performed within AceGen and AceFEM programs. The interested reader is referred to [56, 57].

3 Reference study: size-effects of metamaterial specimens subjected to bending

We investigate here the size-effect phenomena of an assumed metamaterial with fully resolved microstructure. The size-effect phenomena will be analyzed via the effective bending stiffness of beams subjected to pure bending. According to the elementary beam theory, the moment is linked to the curvature by $M(x) = D(x)\kappa(x)$, where $D(x)$ and $\kappa(x)$ are the bending stiffness and the curvature at a position x along the beam. For a constant bending moment $\overline{M}$ along the beam length, we assume an effective flexural rigidity $\overline{D}$ and an effective curvature $\overline{\kappa}$ so that we obtain

$$
\overline{D} = \frac{\overline{M}}{\overline{\kappa}}.
\tag{19}
$$

We design in the following two beams subjected to a vanishing shear force and a constant moment along the length L, see Fig. 2. For the first loading case a rotation θ is applied on the right end while a moment load is enforced for the second loading case instead. A deflection equation $\overline{w}(x)$, which will be fitted later to the heterogeneous beams, featuring an effective constant curvature reads

$$
\overline{w}(x) = \frac{\overline{\kappa}}{2}(x^2 - L^2) \quad \text{satisfying} \quad \overline{w}(L) = 0,
$$
$$
\text{and} \quad \frac{\mathrm{d}\overline{w}(0)}{\mathrm{d}x} = 0,
\tag{20}
$$

A 2D metamaterial is considered with a unit cell consisting of a square with an edge length $l = 1.9 \times 10^{-2}$ m and a circular inclusion at its center with a diameter of $d = 1.2 \times 10^{-2}$ m, see Fig. 3. Both matrix and inclusion are isotropic linear elastic with the material parameters shown in Table 1. The inclusion is 20 times softer than the matrix. A standard triangular finite element with quadratic shape functions (T2) is used for this analysis. The specimens are considered with dimensions $H \times L = n\,l \times 12\,n\,l$ so that the length is always twelve times the height where n is the number of unit cells in the height direction, see Fig. 3.

The boundary condition of the beam models in Fig. 2 are passed on the 2D metamaterial as shown in Fig. 4. For the first loading case we rotate the right edge in plane through a given displacement in x-direction as a linear function of y-coordinates while for the second loading case a moment is applied on the right edge by means of a traction in x-direction as a linear function of y-coordinates. The left boundary for both loading cases is fixed in x-direction and free to move in y-direction. Furthermore, we fix the middle point on the right edge in y-direction. We intend by introducing these two loading cases to prove that they deliver identical results for the microstructured metamaterial beams. This equivalence should then be demonstrated as well by the relaxed micromorphic model when appropriate boundary conditions are set. Furthermore, we assume $\kappa = 1$ and $\bar{t} = 10^9$ N/m.

After solving the fully resolved microstructure, the effective curvature $\overline{\kappa}$ is obtained by the following least square minimization

$$
\sum_{I}^{n_{\text{node}}} ((\boldsymbol{d}_I^u)_2 - \overline{w}(X_I))^2 \to \min,
\tag{21}
$$

which leads, considering Eq. 20, to

$$
\overline{\kappa} = \frac{\sum_{I}^{n_{\text{node}}} (\boldsymbol{d}_I^u)_2 \frac{(X_I)_1^2 - L^2}{2}}{\sum_{I}^{n_{\text{node}}} \left(\frac{(X_I)_1^2 - L^2}{2} \right)^2},
\tag{22}
$$

where X_I and $\boldsymbol{d}_I^u$ are the coordinates and the displacement degrees of freedom at node I. The bending stiffness can be calculated following Eq. 19 where the moment $\overline{M}$ can be calculated using the nodes reactions on the left or right edges. Alternatively, the bending stiffness can be calculated by means of the maximum deflection at the left edge of the beam. We obtain from Eqs. 19 and 20 substituting $x = 0$ and considering $\overline{w}(0) = w^{\text{FEM}}(0)$ since the deflection's fluctuation of the heterogeneous solution is small compared to the maximum deflection

$$
\overline{D} = -\frac{\overline{M}L^2}{2\,w^{\text{FEM}}(0)},
\tag{23}
$$

where $w^{\text{FEM}}(0)$ is the deflection of the FEM solution averaged over the left edge ($x = 0$). Calculating the bending stiffness using Eqs. 19 or 23 delivers the same result which we tested numerically.

The effective material properties of the large specimens can be obtained by the standard computational periodic first-order homogenization produced by a unit cell with periodic boundary condition which is identified as $\mathbb{C}_{\text{macro}}$ in Sect. 4.1. As we will show later the macro elasticity tensor $\mathbb{C}_{\text{macro}}$ is not isotropic and shows cubic symmetry. The size-effects
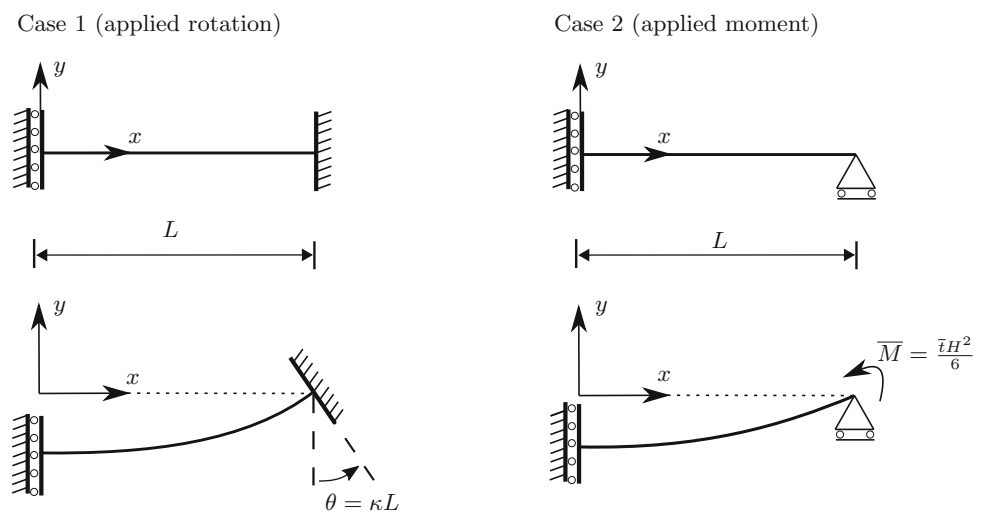
Fig. 2 The beam models, compare Fig. 4

Case 1 (applied rotation)

Case 2 (applied moment)

$\theta = \kappa L$

$\overline{M} = \frac{\overline{t}H^2}{6}$

Table 1 Material parameters of the assumed metamaterial

	Young's modulus: E (GPa)	Poisson's ratio: ν	λ (GPa)	μ (GPa)
Matrix	70	0.333	52.35	26.25
Inclusion	3.5	0.333	2.62	1.31

$H = 5l$

$L = 60\,l \ (800 \cdot 10^3 \text{ finite elements, } 320 \cdot 10^4 \text{ dofs})$

$H = 4l$

$L = 48\,l \ (510 \cdot 10^3 \text{ finite elements, } 205 \cdot 10^4 \text{ dofs})$

$H = 3l$

$L = 36\,l \ (287 \cdot 10^3 \text{ finite elements, } 115 \cdot 10^4 \text{ dofs})$

$H = 2l$

$L = 24\,l \ (128 \cdot 10^3 \text{ finite elements, } 513 \cdot 10^3 \text{ dofs})$

$H = l$

$L = 12\,l \ (32 \cdot 10^3 \text{ finite elements, } 130 \cdot 10^3 \text{ dofs})$
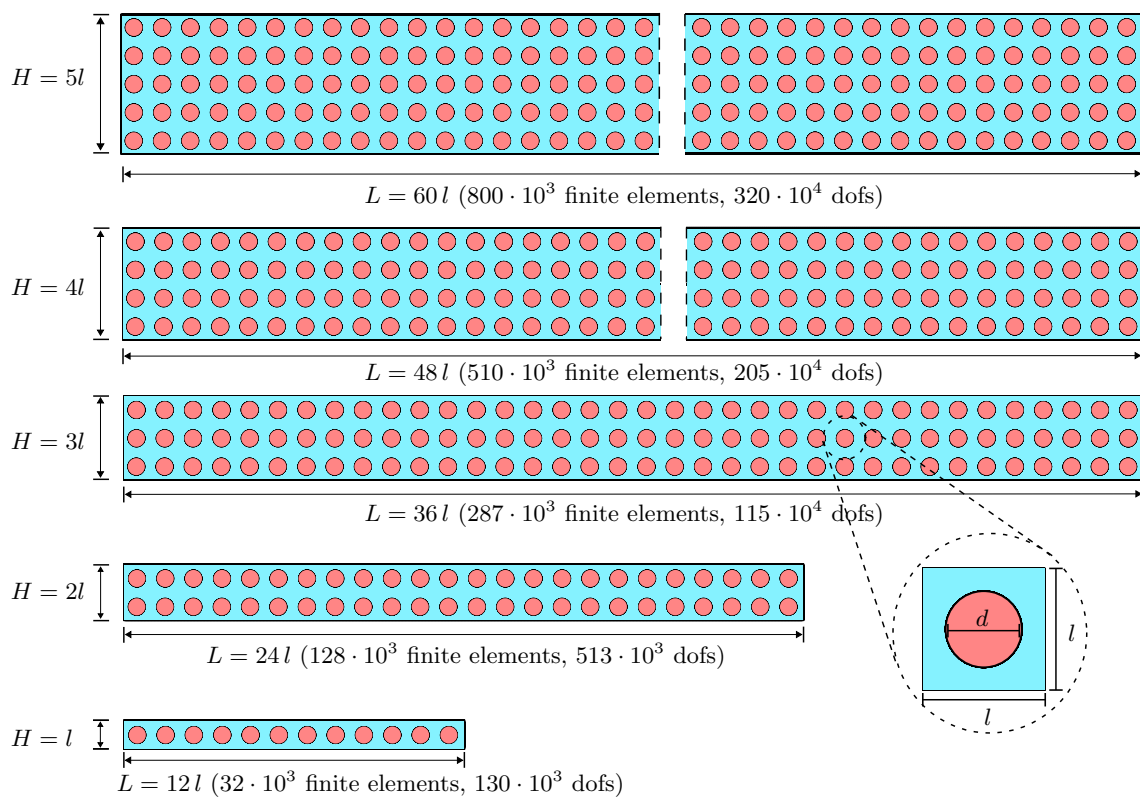
Fig. 3 Illustration shows the geometry of the specimens for $n = 1, 2, 3, 4, 5$ with the assumed unit cell. The number of finite elements with degrees of freedom (dofs) are shown in parentheses
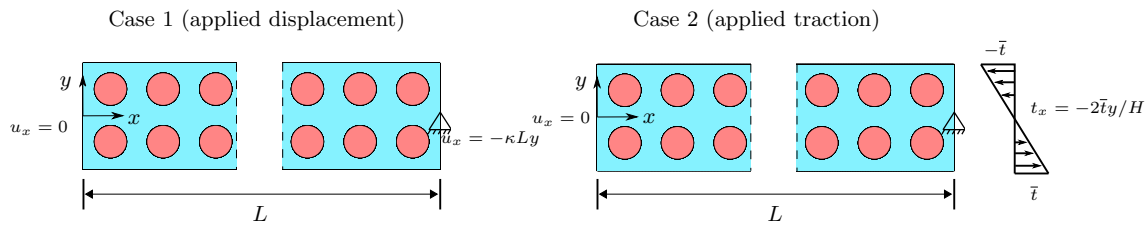
Fig. 4 The boundary conditions of the fully resolved metamaterial shown exemplarily for $n = 2$ ($H \times L = 2l \times 24l$)
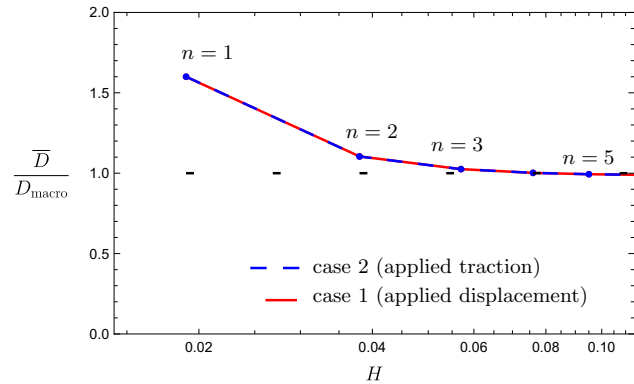
Fig. 5 The normalized bending stiffness varying the beam size $H \times L = nl \times 12nl$

are shown via the so-called normalized bending stiffness $\overline{D}/D_{\mathrm{macro}}$ plotted in Fig. 5 which relates the actual stiffness of the fully discretized metamaterial to the one obtained from homogenized linear elasticity with $\mathbb{C}_{\mathrm{macro}}$ which reads analytically

$$D_{\mathrm{macro}} = \frac{E_{\mathrm{macro}} H^3}{12(1 - \nu_{\mathrm{macro}}^2)}. \tag{24}$$

The normalized bending stiffness approaches the value one when we increase the specimen size. Applying a rotation (loading case 1) or a moment (loading case 2) leads to similar results as expected.

4 Size-effects of the relaxed micromorphic continuum subjected to pure bending

The previous size-effects exhibited by the fully resolved heterogeneous material should be reproduced by the relaxed micromorphic model. However, the boundary conditions and material parameters identification are not obvious.

4.1 Identification of $\mathbb{C}_{\mathbf{macro}}$

The macro elasticity tensor $\mathbb{C}_{\mathrm{macro}}$ corresponds to the case $L_c \to 0$ equivalent to large values of n where the macro homogeneous response is expected. A unit cell with periodic

boundary conditions should be used, see for example [126]. The geometry of the unit cell has no role for this standard analysis. Our analysis shows that $\mathbb{C}_{\mathrm{macro}}$ has the cubic symmetry property for our assumed metamaterial and it reads in Voigt notation

$$\mathbb{C}_{\mathrm{macro}} = \begin{pmatrix} 2\mu_{\mathrm{macro}} + \lambda_{\mathrm{macro}} & \lambda_{\mathrm{macro}} & 0 \\ \lambda_{\mathrm{macro}} & 2\mu_{\mathrm{macro}} + \lambda_{\mathrm{macro}} & 0 \\ 0 & 0 & \mu_{\mathrm{macro}}^* \end{pmatrix}, \tag{25}$$

where three parameters need to be defined. We obtain by our standard numerical analysis

$$\mathbb{C}_{\mathrm{macro}} = \begin{pmatrix} 47.86 & 17.61 & 0 \\ 17.61 & 47.86 & 0 \\ 0 & 0 & 9.98 \end{pmatrix} [\mathrm{GPa}]$$

$$\Rightarrow \quad \begin{aligned} \lambda_{\mathrm{macro}} &= 17.61 \text{ GPa} \\ \mu_{\mathrm{macro}} &= 15.13 \text{ GPa}. \\ \mu_{\mathrm{macro}}^* &= 9.98 \text{ GPa} \end{aligned} \tag{26}$$

4.2 Identification of $\mathbb{C}_{\mathbf{micro}}$ (first approach)

The micro elasticity tensor $\mathbb{C}_{\mathrm{micro}}$ in the relaxed micromorphic model is identified as the maximum stiffness on the micro-scale which must exhibit the cubic symmetry similar to $\mathbb{C}_{\mathrm{macro}}$ according to the extended Neumanns's principle [81]. In order to achieve stiff estimates for $\mathbb{C}_{\mathrm{micro}}$ we apply first affine Dirichlet boundary conditions. Furthermore, we have to choose unit cells which preserve the cubic symmetry under the applied Dirichlet boundary conditions. However, different variants of unit cells must be investigated for the affine Dirichlet boundary conditions. For each choice of a unit cell $i = 1, \ldots, r$ with the affine Dirichlet boundary conditions, we obtain the corresponding apparent stiffness tensor denoted as $\mathbb{C}_i^{\mathrm{D}}$. The positive definite micro elasticity tensor will be set as the least upper bound of the apparent stiffness of the microstructure measured in the energy norm following the Löwner matrix supremum problem, see for details [81].

For the assumed metamaterial, four different variants of the unit cell are suitable, see Fig. 6, which lead to the elasticity tensors $\mathbb{C}_i^{\mathrm{D}}$, $i = 1, \ldots, 4$ with the cubic symmetry property as intended. The results are summarized in Table 2.

Fig. 6 The possible choices of the unit cells with cubic symmetry. The edge length of the unit cell equals to l for (1) and (2) and $\sqrt{2}\,l$ for (3) and (4)
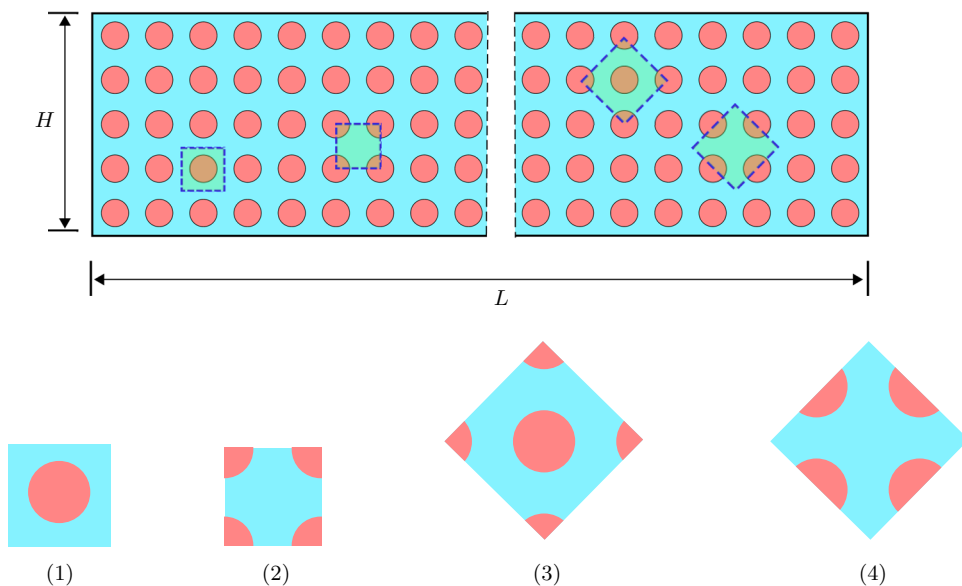

Table 2 The elasticity parameters of the unit cells in Fig. 6 under affine Dirichlet boundary conditions

Unit cell	λ_i (GPa)	μ_i (GPa)	μ_i^* (GPa)
1	18.26	15.34	**14.61**
2	**20.15**	**15.83**	14.44
3	19.25	15.54	13.19
4	19.56	15.66	12.68

The elasticity parameters define elasticity tensors which exhibit cubic symmetry similar to $\mathbb{C}_{\text{macro}}$

The micro elasticity tensor $\mathbb{C}_{\text{micro}}^{L\ddot{o}wner}$ is defined then by the Löwner matrix supremum problem as

$$\tilde{\boldsymbol{\varepsilon}} : \mathbb{C}_{\text{micro}}^{L\ddot{o}wner} : \tilde{\boldsymbol{\varepsilon}} \geq \tilde{\boldsymbol{\varepsilon}} : \mathbb{C}_i^{\text{D}} : \tilde{\boldsymbol{\varepsilon}} \quad \text{where}$$
$$\mathrm{i} = 1, \dots, 4 \quad, \quad \forall \tilde{\boldsymbol{\varepsilon}} \in \text{Sym}(3). \tag{27}$$

which turns for the cubic symmetry case to the following one written in Voigt notation

$$\begin{pmatrix} \tilde{\varepsilon}_{11} \\ \tilde{\varepsilon}_{22} \\ 2\tilde{\varepsilon}_{12} \end{pmatrix} : \begin{pmatrix} 2\mu_{\text{micro}}^{L\ddot{o}wner} + \lambda_{\text{micro}}^{L\ddot{o}wner} & \lambda_{\text{micro}}^{L\ddot{o}wner} & 0 \\ \lambda_{\text{micro}}^{L\ddot{o}wner} & 2\mu_{\text{micro}}^{L\ddot{o}wner} + \lambda_{\text{micro}}^{L\ddot{o}wner} & 0 \\ 0 & 0 & (\mu^*)_{\text{micro}}^{L\ddot{o}wner} \end{pmatrix} : \begin{pmatrix} \tilde{\varepsilon}_{11} \\ \tilde{\varepsilon}_{22} \\ 2\tilde{\varepsilon}_{12} \end{pmatrix} \geq$$
$$\begin{pmatrix} \tilde{\varepsilon}_{11} \\ \tilde{\varepsilon}_{22} \\ 2\tilde{\varepsilon}_{12} \end{pmatrix} : \begin{pmatrix} 2\mu_i + \lambda_i & \lambda_i & 0 \\ \lambda_i & 2\mu_i + \lambda_i & 0 \\ 0 & 0 & \mu_i^* \end{pmatrix} : \begin{pmatrix} \tilde{\varepsilon}_{11} \\ \tilde{\varepsilon}_{22} \\ 2\tilde{\varepsilon}_{12} \end{pmatrix} \tag{28}$$
$$\text{for } i = 1, \dots, 4 \quad, \forall \begin{pmatrix} \tilde{\varepsilon}_{11} \\ \tilde{\varepsilon}_{22} \\ \tilde{\varepsilon}_{12} \end{pmatrix} \in \mathbb{R}^3.$$

The solution of the previous problem reads

$$(\mu^*)_{\text{micro}}^{L\ddot{o}wner} \geq \max_i\{\mu_i^*\}, \quad \mu_{\text{micro}}^{L\ddot{o}wner} \geq \max_i\{\mu_i\},$$
$$\lambda_{\text{micro}}^{L\ddot{o}wner} + \mu_{\text{micro}}^{L\ddot{o}wner} \geq \max_i\{\mu_i + \lambda_i\}, \tag{29}$$

for $i = 1, \dots, 4$. We take therefore (see Table 2)

$$(\mu^*)_{\text{micro}}^{L\ddot{o}wner} := \mu_1^* = 14.61\,\text{GPa},$$
$$\mu_{\text{micro}}^{L\ddot{o}wner} := \mu_2 = 15.83\,\text{GPa}, \tag{30}$$
$$\lambda_{\text{micro}}^{L\ddot{o}wner} := \mu_2 + \lambda_2 - \mu_{\text{micro}}^{L\ddot{o}wner} = 20.15\,\text{GPa},$$

and thus

$$\mathbb{C}_{\text{micro}}^{L\ddot{o}wner} := \begin{pmatrix} 51.81 & 20.15 & 0 \\ 20.15 & 51.81 & 0 \\ 0 & 0 & 14.61 \end{pmatrix} [\text{GPa}]. \tag{31}$$

However, the previous estimate will serve as a lower bound for $\mathbb{C}_{\text{micro}}$. In Fig. 7, we show the size-effect of the fully resolved metamaterial beams and the linear elasticity solutions with different elasticity tensors: (I) $\mathbb{C}_{\text{macro}}$, (II) $\mathbb{C}_{\text{micro}}^{L\ddot{o}wner}$, (III) $\mathbb{C}_{\text{matrix}}$ of the homogeneous isotropic matrix, and (IV) $\mathbb{C}_{\text{Voigt}}$ which is isotropic and obtained by the equal strain assumption $\mathbb{C}_{\text{Voigt}} = \phi_{\text{matrix}}\mathbb{C}_{\text{matrix}} + \phi_{\text{inclusion}}\mathbb{C}_{\text{inclusion}}$ where ϕ_{matrix} and $\phi_{\text{inclusion}}$ are the volume fractions of the matrix and inclusion, respectively, which leads to $\lambda_{\text{Voigt}} = 36.77\,\text{GPa}$ and $\mu_{\text{Voigt}} = 18.44\,\text{GPa}$. The calculated value for $\mathbb{C}_{\text{micro}}^{L\ddot{o}wner}$ is too soft compared to the microstructured beams and even linear elasticity with $\mathbb{C}_{\text{Voigt}}$ is softer than the solution of the fully resolved metamaterial beam for $n = 1$. This can be explained by the fact that the typical bending mode, e.g. due to a pure bending moment as in the paper, cannot be mapped with affine Dirichlet Boundary conditions. Here, a "Voigt bound" for higher modes (not for affine deformations) would be required, which, to our knowledge, does not exist. Note that the tensor $\mathbb{C}_{\text{micro}}$, although appearing in the relaxed micromorphic model and in the classical micromorphic model, does not have the same meaning in the latter,

Fig. 7 The normalized bending stiffness varying the beam size $H \times L = n\, l \times 12\, n\, l$ compared to the ones obtained by linear elasticity with different elasticity tensors shown in Sect. 4.2
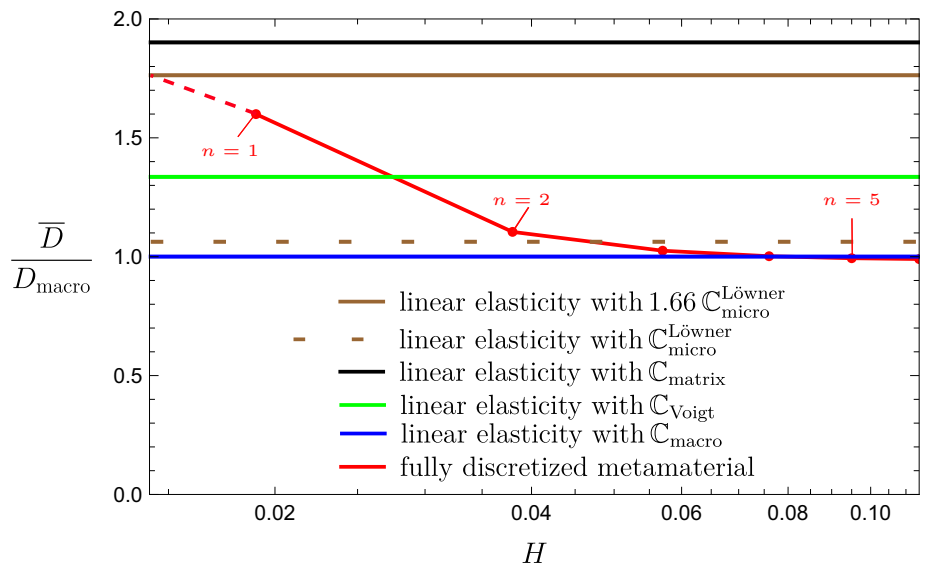

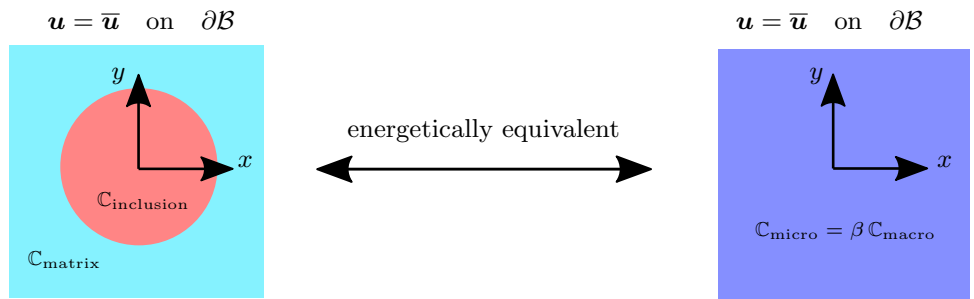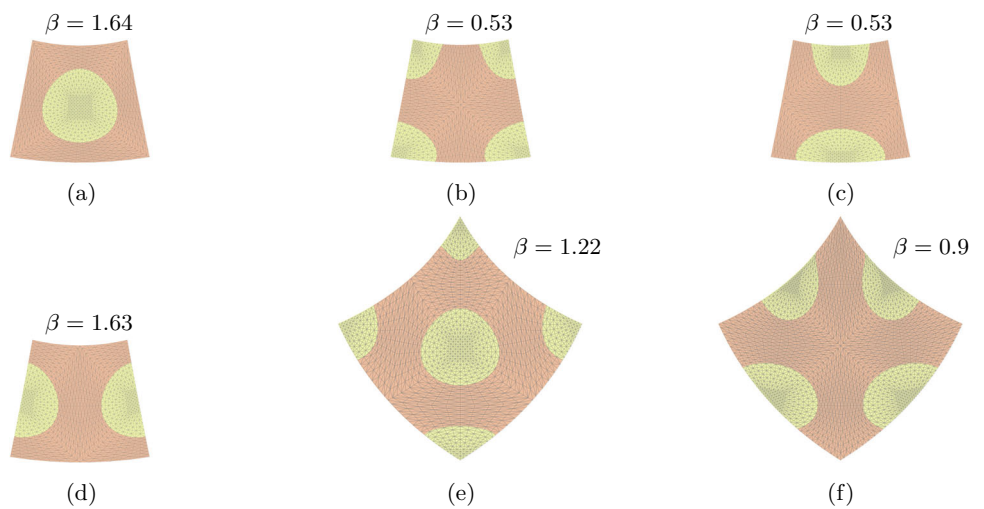**Fig. 8** Illustration shows the procedure used to calculate β

Fig. 9 The values of the parameter β calculated for different unit cells. Unit cell (**a**) provides the stiffest flexural stiffness with $\beta = 1.64$

which is related to the bounded stiffness property of the former. Since $\mathbb{C}_{\text{matrix}}$ represents the largest stiffness, we may relate $\mathbb{C}_{\text{micro}}$ to the matrix stiffness $\mathbb{C}_{\text{matrix}}$ and introduce a scalar $\alpha \geq 1$ so that we have $\mathbb{C}_{\text{micro}} := \alpha\, \mathbb{C}_{\text{micro}}^{L\ddot{o}wner}$. We define an upper limit for $\mathbb{C}_{\text{micro}}$ as

$$\tilde{\boldsymbol{\varepsilon}} : \mathbb{C}_{\text{matrix}} : \tilde{\boldsymbol{\varepsilon}} \geq \tilde{\boldsymbol{\varepsilon}} : \mathbb{C}_{\text{micro}} : \tilde{\boldsymbol{\varepsilon}}$$
$$= \tilde{\boldsymbol{\varepsilon}} : \alpha\, \mathbb{C}_{\text{micro}}^{L\ddot{o}wner} : \tilde{\boldsymbol{\varepsilon}}, \quad \forall \tilde{\boldsymbol{\varepsilon}} \in \text{Sym}(3). \tag{32}$$
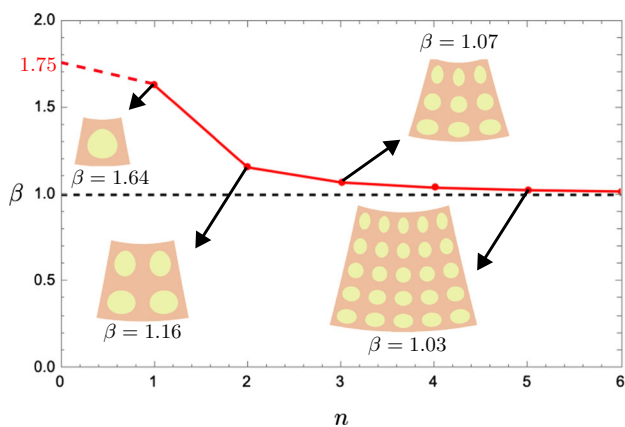
Fig. 10 The parameter β converges to the value one when increasing the size of a cluster of unit cells ($n \times n$) shown exemplarily for type (**a**) in Fig. 9. We also show the extrapolated value $\beta = 1.75$
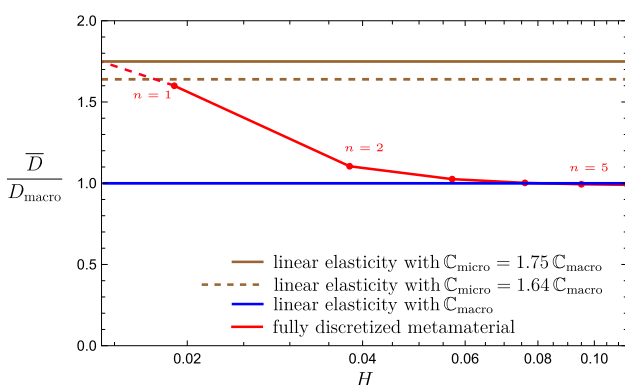

Fig. 11 The normalized bending stiffness varying the beam size $H \times L = n\,l \times 12\,n\,l$ compared to the ones obtained by linear elasticity with different elasticity tensors shown in Sect. 4.3

By introducing Eq. 32 we keep the anisotropic symmetry property of $\mathbb{C}_{\text{micro}}$ while the elasticity tensor $\mathbb{C}_{\text{matrix}}$ is isotropic. We obtain then

$$\mu^*_{\text{matrix}} = \mu_{\text{matrix}} \geq \alpha(\mu^*)^{L\ddot{o}wner}_{\text{micro}}, \quad \mu_{\text{matrix}} \geq \alpha\mu^{L\ddot{o}wner}_{\text{micro}},$$
$$\lambda_{\text{matrix}} + \mu_{\text{matrix}} \geq \alpha(\lambda^{L\ddot{o}wner}_{\text{micro}} + \mu^{L\ddot{o}wner}_{\text{micro}}), \quad (33)$$

which leads to

$$\alpha \in [1, \min(\frac{\mu^*_{\text{matrix}}}{(\mu^*)^{L\ddot{o}wner}_{\text{micro}}}, \frac{\mu_{\text{matrix}}}{\mu^{L\ddot{o}wner}_{\text{micro}}}, \frac{\mu_{\text{matrix}} + \lambda_{\text{matrix}}}{\mu^{L\ddot{o}wner}_{\text{micro}} + \lambda^{L\ddot{o}wner}_{\text{micro}}})]$$
$$= [1, 1.66]. \quad (34)$$

Figure 7 shows that linear elasticity with $\mathbb{C}_{\text{micro}} = 1.66\,\mathbb{C}^{L\ddot{o}wner}_{\text{micro}}$ is stiffer than the fully resolved metamateriel for $n = 1$ and therefore it is a valid choice. However, assuming $\mathbb{C}_{\text{micro}} = \mathbb{C}_{\text{matrix}}$ does not break the extended Neumann's principle. We will investigate later numerically the consequences of the different choices for $\mathbb{C}_{\text{micro}}$.

4.3 Identification of $\mathbb{C}_{\text{micro}}$ (second approach)

The affine Dirichlet boundary conditions are unable to capture the size-effects as we have shown in Sect. 4.2. In order to estimate the stiffness $\mathbb{C}_{\text{micro}}$ for the relaxed micromorphic model we choose in the following approach the most simple ansatz

$$\mathbb{C}_{\text{micro}} = \beta\,\mathbb{C}_{\text{macro}} \quad \text{with} \quad \beta > 1. \quad (35)$$

In general, the size dependency cannot be modeled by a single scalar β alone, of course. We introduce this numerical study to get a first estimate. The parameter β is determined via the energy equivalence of a heterogeneous microstructured domain and an equivalent homogeneous domain with the same dimensions governed by linear elasticity with elasticity tensor $\mathbb{C}_{\text{micro}} = \beta\,\mathbb{C}_{\text{macro}}$, see Fig. 8. We consider here a higher-order deformation mode which is the bending mode. The bending mode is enforced by applying non-affine Dirichlet boundary conditions on the whole boundary. They are derived from the analytical solution of the pure bending problem of the homogeneous problem in [86]

$$\boldsymbol{u} = \overline{\boldsymbol{u}} = \frac{\kappa}{2} \begin{pmatrix} -2\,x\,y \\ \dfrac{\lambda_{\text{macro}}}{2\mu_{\text{macro}} + \lambda_{\text{macro}}}y^2 + x^2 \end{pmatrix} \quad \text{on} \quad \partial\mathcal{B}, \quad (36)$$

which leads to a constant curvature κ for the homogeneous case with no shear strain and one active stress component σ_{11}

$$\overline{\boldsymbol{\varepsilon}} = \text{sym}\,\nabla\overline{\boldsymbol{u}} = \begin{pmatrix} -\kappa\,y & 0 \\ 0 & \dfrac{\lambda_{\text{macro}}\kappa\,y}{2\mu_{\text{macro}} + \lambda_{\text{macro}}} \end{pmatrix},$$
$$\overline{\boldsymbol{\sigma}} = \begin{pmatrix} \dfrac{-4\mu_{\text{macro}}(\mu_{\text{macro}} + \lambda_{\text{macro}})\beta\kappa\,y}{2\mu_{\text{macro}} + \lambda_{\text{macro}}} & 0 \\ 0 & 0 \end{pmatrix}. \quad (37)$$

We search for the stiffest possible component on the microstructure under flexural deformation mode (highest values of β) by investigating different arrangements of unit cells. Six different arrangements were considered, see Fig. 9. The largest obtained value is $\beta = 1.64$. Increasing the size of the arrangements of the unit cells, considered in Fig. 9, we retrieve the macro property where β converges to the value one as it should. This behavior is shown exemplarily for unit cell (a) in Fig. 10.

The choice $\mathbb{C}_{\text{micro}} = 1.64\,\mathbb{C}_{\text{macro}}$ guarantees that a homogeneous continuum with elasticity tensor $\mathbb{C}_{\text{micro}} = 1.64\,\mathbb{C}_{\text{macro}}$ is stiffer than the fully discretized metamaterial. In Fig. 11, we show the size-effect of the fully resolved metamaterial beams and the linear elasticity solutions with elasticity tensors $\mathbb{C}_{\text{micro}} = 1.64\,\mathbb{C}_{\text{macro}}$ and $\mathbb{C}_{\text{macro}}$. The upper limit $\mathbb{C}_{\text{micro}} = 1.64\,\mathbb{C}_{\text{macro}}$ is slightly stiffer than the relatively

Case 1 (applied displacement)   Case 2 (applied traction)
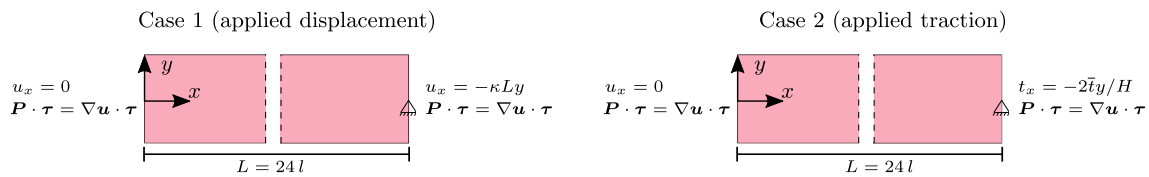

Fig. 12 The boundary value problems of the homogeneous relaxed micromorphic model for both loading cases. These boundary value problems are equivalent to the two cases of the heterogeneous metamaterial shown in Fig. 4. The upper and lower edges are traction-free
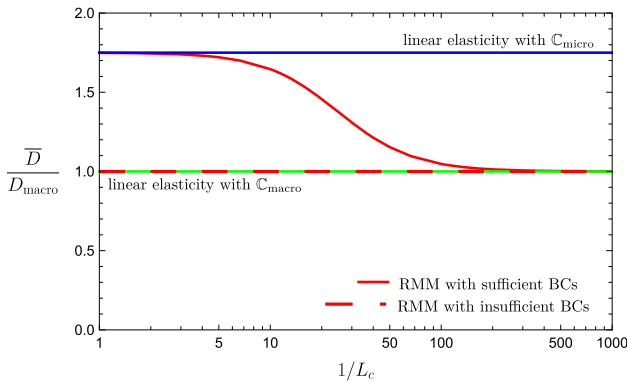

Fig. 13 The normalized bending stiffness obtained by the relaxed micromorphic model for both loading cases assuming $\mathbb{C}_c = \mathbf{0}\,(\mu_c = 0)$ while varying the characteristic length L_c. Sufficient BCs indicate to apply the consistent coupling condition on the left and right edges, see Fig. 12. Removing the consistent coupling condition on left or right edge is considered as insufficient and leads to no size-effect

stiffest metamaterial beam ($n = 1$) which confirms its validity. However, to provide a better fitting, we extrapolate $\mathbb{C}_{\mathrm{micro}} = 1.75\,\mathbb{C}_{\mathrm{macro}}$ as an improved upper bound. Unique identification of the micro elasticity tensor $\mathbb{C}_{\mathrm{micro}}$ remains an open question for future works.

4.4 Identification of $\mathbb{C}_e$

The elasticity tensor $\mathbb{C}_e$ is calculated via the micro–macro Reuss-like homogenization formula

$$\mathbb{C}_{\mathrm{macro}}^{-1} = \mathbb{C}_{\mathrm{micro}}^{-1} + \mathbb{C}_e^{-1}$$
$$\Rightarrow \quad \mathbb{C}_e = \mathbb{C}_{\mathrm{micro}}(\mathbb{C}_{\mathrm{micro}} - \mathbb{C}_{\mathrm{macro}})^{-1}\mathbb{C}_{\mathrm{macro}}. \quad (38)$$

The obtained elasticity tensor $\mathbb{C}_e$ is automatically positive definite since $\mathbb{C}_{\mathrm{micro}} > \mathbb{C}_{\mathrm{macro}}$ and has cubic symmetry property. However, no obvious physical interpretation can be assigned to the tensor $\mathbb{C}_e$.

4.5 The boundary conditions of the micro-distortion field

The boundary conditions (BCs) of the micro-distortion field are key components for the relaxed micromorphic model. The boundary conditions should be chosen in a way that

induces a curvature in the model, i.e. Curl $\mathbf{P} \neq \mathbf{0}$. Otherwise, insufficient boundary condition of the micro-distortion field can cause unwanted behavior of the relaxed micromorphic model. This behavior is represented by showing no size-effects or not reaching the intended upper limit (linear elasticity with $\mathbb{C}_{\mathrm{micro}}$) for $L_c \to \infty$.

4.5.1 Symmetric force stress case

We assume here $\mathbb{C}_c = 0$ which causes symmetric force stress $\boldsymbol{\sigma}$ and symmetric Curl $\mathbf{m}$ because Eq. 9d becomes symmetric. We test the sufficiency of the boundary condition by comparing the solution of the relaxed micromorphic model for varied values of the characteristic length with the solutions obtained by the standard linear elasticity with elasticity tensors $\mathbb{C}_{\mathrm{micro}}$ and $\mathbb{C}_{\mathrm{macro}}$. More specifically, the relaxed micromorphic model should reproduce linear elasticity with elasticity tensors $\mathbb{C}_{\mathrm{micro}}$ and $\mathbb{C}_{\mathrm{macro}}$ for $L_c \to \infty$ and $L_c \to 0$, respectively, see [26, 85–87, 89, 100].

We design a test by fixing the geometry $H \times L = 2\,l \times 24\,l$ with assuming $\mathbb{C}_{\mathrm{micro}} = 1.75\,\mathbb{C}_{\mathrm{macro}}$ and setting $\mu = \mu_{\mathrm{macro}}$. The boundary conditions of the displacement field are taken similar to the ones applied on the fully resolved metamaterials in Fig. 4. For the first case with applied rotation, the consistent coupling condition is applied on the right and left edges via a penalty approach, see Fig. 12. Indeed, applying the consistent coupling condition on the Dirichlet boundary of the displacement field is adequate to fulfill the theoretical limits of the relaxed micromorphic model. Removing the consistent coupling condition on left or right edges leads to vanishing curvature and turns the relaxed micromorphic model into standard linear elasticity with $\mathbb{C}_{\mathrm{macro}}$. The previous behavior is demonstrated in Fig. 13. The exact same behavior is observed for the second loading case with applied traction if we apply the consistent coupling condition on the boundary corresponding to the first loading case, see Fig. 12. Consequently, the relaxed micromorphic model results in consistent results for both loading cases, see Fig. 13.

4.5.2 Non-symmetric force stress case

Here, we assume $\mathbb{C}_c = 2\mu_c \mathbb{I}$ where $\mathbb{I}$ is the fourth order identity tensor and μ_c is the Cosserat couple modulus acting as a spring constant between the skew-symmetric parts of $\nabla \boldsymbol{u}$

and P. We study the influence of varying the Cosserat couple modulus $\mu_c \in [0, 0.01, 0.1, 1] * \mu_{\text{macro}}$ considering different scenarios of the boundary condition of P. The geometry and the remaining material parameters are taken as for the symmetric case, see Sect. 4.5.1.

In Fig. 14, we show the normalized bending stiffness for the cases (a) the consistent coupling condition is applied either on the left or right edge, (b) no consistent boundary condition is considered and (c) the consistent coupling condition is applied on both left and right edges. Size-effects are noticed even if the consistent coupling condition is not placed on the right and left edges simultaneously which is not the case for the symmetric force case ($\mu_c = 0$). Increasing the Cosserat couple modulus μ_c raises the stiffness of the relaxed micromorphic model closer to linear elasticity with $\mathbb{C}_{\text{micro}}$ for $L_c \to \infty$ and even reach it in Fig. 14a. However, it is not guaranteed that the relaxed micromorphic model achieves linear elasticity with $\mathbb{C}_{\text{micro}}$ for $L_c \to \infty$, see Fig. 14b. The results of enforcing the consistent coupling condition on both left and right edges are equivalent for the symmetric and non-symmetric cases in Figs. 13 and 14c, respectively, and the Cosserat couple modulus has no influence.

4.5.3 Cosserat limit, special case of a skew-symmetric micro-distortion field

For the case of $\mathbb{C}_{\text{micro}} \to \infty$, the micro-distortion field P must be skew-symmetric and the Cosserat model is recovered, c.f. [10, 21, 41, 53]. We investigate here the influence of different scenarios of the boundary conditions for the micro-distortion field P similar to Sect. 4.5.2: (a) the consistent coupling condition is applied on either the left or right edge, (b) without enforcing the consistent boundary condition and (c) the consistent coupling condition is applied on both left and right edges for $\mathbb{C}_{\text{micro}} = 1000 \, \mathbb{C}_{\text{macro}}$. Different values of the Cosserat couple modulus μ_c are assumed for varied values of the characteristic length L_c in Fig. 16. Our analysis shows that when the consistent coupling condition is not applied at both right and left ends, large values of L_c result in a beam that does not bend (Fig. 15), causing a nonphysical bending stiffness. This highlights the crucial role of the consistent coupling condition, not just in the relaxed micromorphic model, but also in the Cosserat case. Hence due to the bending stiffness issue, we have opted to show the relative total energy Π/Π_{macro} for this analysis alternatively.

We notice that linear elasticity with elasticity tensor $\mathbb{C}_{\text{micro}}$ is recognized as an upper limit only when the consistent coupling condition is enforced on both left and right edges in Fig. 16c. Weak size-effects are noticed when the consistent coupling condition is not enforced, Fig. 16a, b. While size-effects are prompted only for non-vanishing Cosserat couple modulus $\mu_c \neq 0$ for cases (a) and (b), enforcing the consistent coupling condition on both left and right edges

simultaneously allows the model to act on the intended theoretical range with no influence of the Cosserat couple modulus μ_c which is well known for the Cosserat model. This can be explained by the fact that the skew-symmetric part of the micro-distortion field is the same as the skew-symmetric part of the gradient of the displacement, see [86], which is the case for both the relaxed micromorphic continuum in Fig. 14c and the Cosserat model in Fig. 16c.

4.6 Scaling of the curvature

The curvature for the 2D case is isotropic because Curl P is reduced to a vector. Therefore, the curvature will be controlled by only one parameter with assuming that $\mathbb{L} = \mathbb{I}$ is the fourth order identity tensor. Since the parameters μ and L_c should be set constant independent of the specimen size, the curvature is modified by incorporating the size of the beams through the number n. Figure 5 shows that stiffer response is observed for smaller values of the number n ($n = 1$ is the stiffest). The relaxed micromorphic model exhibits stiffer response for bigger values of the characteristic length L_c (inversely proportional to n), see for example Fig. 13. Therefore, we replace the last term in Eq. 2 by

$$\frac{1}{2} \mu \left(\frac{L_c}{n} \right)^2 \text{Curl} P : \text{Curl} P, \tag{39}$$

where n denotes the number of unit cells in the second-direction. Hence, for a constant L_c smaller values are obtained for the term L_c/n by increasing the beam size (increasing n) which reproduces the intended size-effects (smaller is stiffer). This modification is not ad hoc, but follows from a rigorous scaling argument, c.f. [81] and applies as such to higher-gradient models or the classical micromorphic model as well. Note that the shear modulus μ appears for dimensional reasons and is a priori not related to the shear moduli appearing in $\mathbb{C}_{\text{macro}}$ or $\mathbb{C}_{\text{micro}}$.

5 Final calibration

Now, we provide an identification scheme for the scale-independent material parameters of the relaxed micromorphic model. The boundary conditions of the micro-distortion field are determined in order to guarantee the intended behavior of the relaxed micromorphic model and the influence of the characteristic length L_c for both loading cases. For this calibration we assume symmetric force stress, i.e. $\mathbb{C}_c = \mathbf{0}$. As we discussed in Sects. 4.2, 4.3 and 4.5.3, different choices can be made for $\mathbb{C}_{\text{micro}}$, e.g. $\mathbb{C}_{\text{micro}} = 1.66 \, \mathbb{C}_{\text{micro}}^{L\ddot{o}wner}$, $\mathbb{C}_{\text{micro}} = \mathbb{C}_{\text{matrix}}$, $\mathbb{C}_{\text{micro}} = 1.75 \, \mathbb{C}_{\text{macro}}$ and $\mathbb{C}_{\text{micro}} = 1000 \, \mathbb{C}_{\text{macro}}$. Considering $\mathbb{C}_{\text{micro}} = 10,000 \, \mathbb{C}_{\text{macro}}$ yield similar results to $\mathbb{C}_{\text{micro}} = 1000 \, \mathbb{C}_{\text{macro}}$, as expected, which can be explained
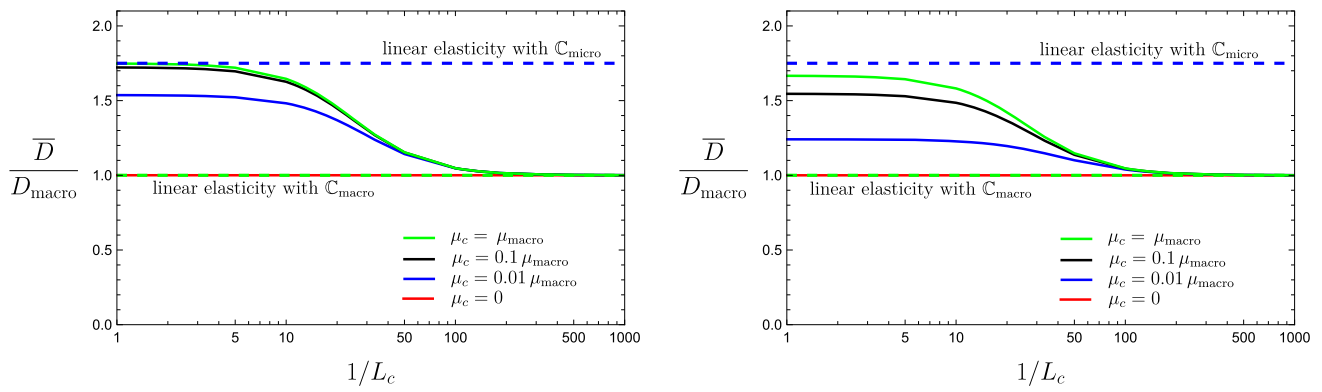
(a) consistent coupling condition either on the left or right edge

(b) no consistent coupling condition
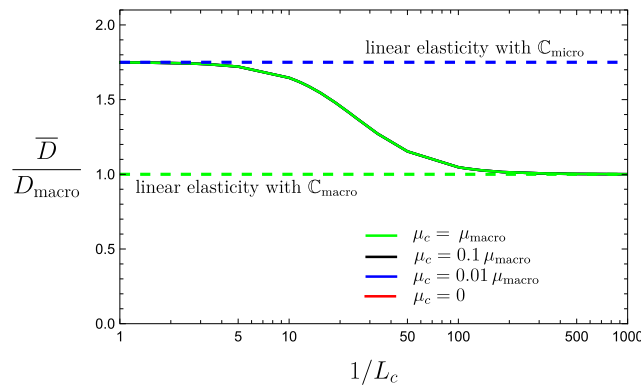
(c) consistent coupling condition on the left and right edges

Fig. 14 The normalized bending stiffness obtained by the relaxed micromorphic model for both loading cases with non-symmetric force stress and with varying the characteristic length L_c. Different scenarios are investigated for the boundary conditions of the micro-distortion field
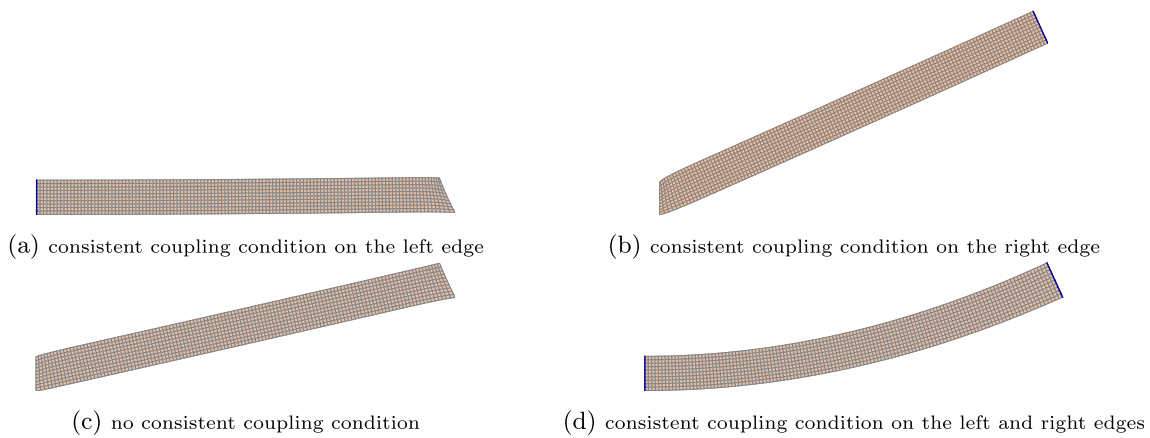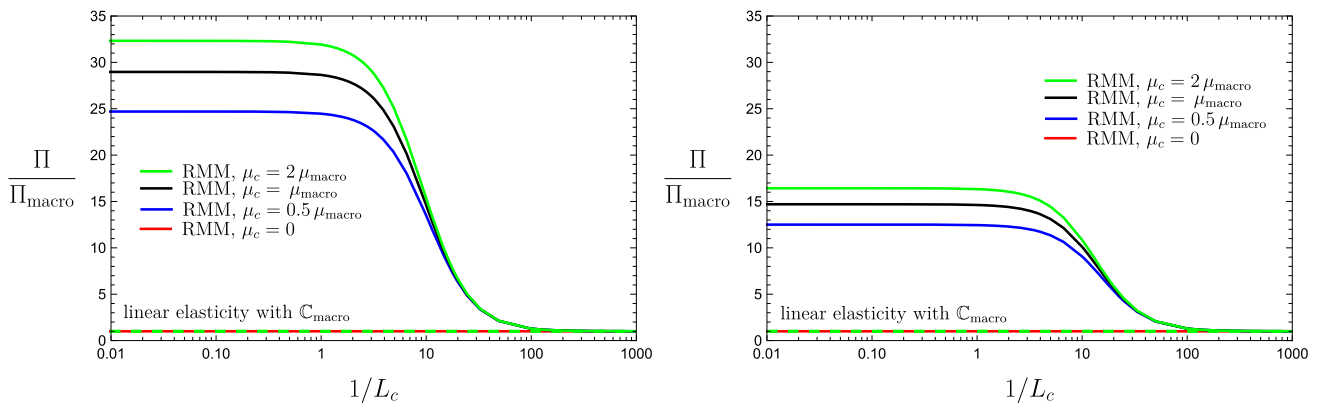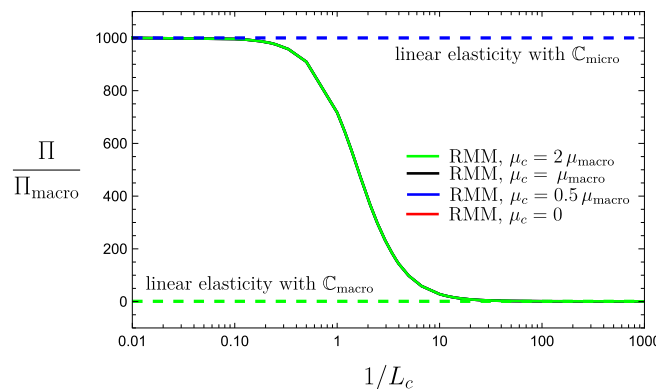

(a) consistent coupling condition on the left edge

(b) consistent coupling condition on the right edge

(c) no consistent coupling condition

(d) consistent coupling condition on the left and right edges

Fig. 15 The deformed beams for the case $\mathbb{C}_{\mathrm{micro}} = 1000\,\mathbb{C}_{\mathrm{macro}}$ "Cosserat type" with $L_c = 1000\,\mathrm{m}$ and $\mu_c = 2\,\mu_{\mathrm{macro}}$. Bending of the beam can only be induced when the consistent coupling condition is applied on both its left and right ends

(a) consistent coupling condition either on the left or right edge

(b) no consistent coupling condition

(c) consistent coupling condition on the left and right edges

Fig. 16 The relative total energy obtained by the relaxed micromorphic model for both loading cases with non-symmetric force stress and with varying the characteristic length L_c. Here, we assume $\mathbb{C}_{\text{micro}} = 1000\,\mathbb{C}_{\text{macro}}$ leading to a skew-symmetric micro-distortion field which retrieves the Cosserat model since the curvature expression is then equivalent with the Cosserat framework, see [41]. Different scenarios are investigated for the boundary conditions of the micro-distortion field

by the fact that we are operating in a range close to the lower bound $\mathbb{C}_{\text{macro}}$. For each choice of $\mathbb{C}_{\text{micro}}$, the curvature should be calibrated by means of L_c and μ. Without loss of generality, we can always assume the shear modulus $\mu = \mu_{\text{macro}}$ and then the characteristic length L_c should be selected in order to capture the size-effects of the fully discretized metamaterial, Fig. 17. Alternatively, the characteristic length L_c can be set in advance, e.g. $L_c = l$, and then the shear modulus μ should be calibrated, see Fig. 18 and Eq. 39. The decisive quantity is the product μL_c^2. Since the Cosserat curvature coincides with the curvature expression of the relaxed micromorphic model [41], one would expect that using similar values for μL_c^2 is a sensible choice. As Figs. 17d and 18d show, this is not the case. For a rough Cosserat fit different orders of magnitude for μL_c^2 have to be taken which are getting arbitrary. Furthermore, the data points can be fitted also with a Cosserat type model but it should be remarked that the unbounded stiffness (beyond $n = 1$) leads to a sensitive identification

of the parameters. The same problem would appear by using second gradient or the classical micromorphic theories.

6 Validation: further numerical examples

This study assesses the obtained material parameters of the relaxed micromorphic model for two additional loading scenarios apart from the pure bending. The fully discretized metamaterial samples considered have the dimensions and material parameters as outlined before in Sect. 3. In the relaxed micromorphic model, we consider the symmetric case where $\mu_c = 0$. The macro-scale elasticity tensor, $\mathbb{C}_{\text{macro}}$, is defined in Sect. 4.1 and the curvature is scaled to the specimen's size using Eq. 39 under the assumption of $\mu = \mu_{\text{macro}}$. The micro-scale elasticity tensor will be determined using the same four different assumptions outlined in Sect. 5.
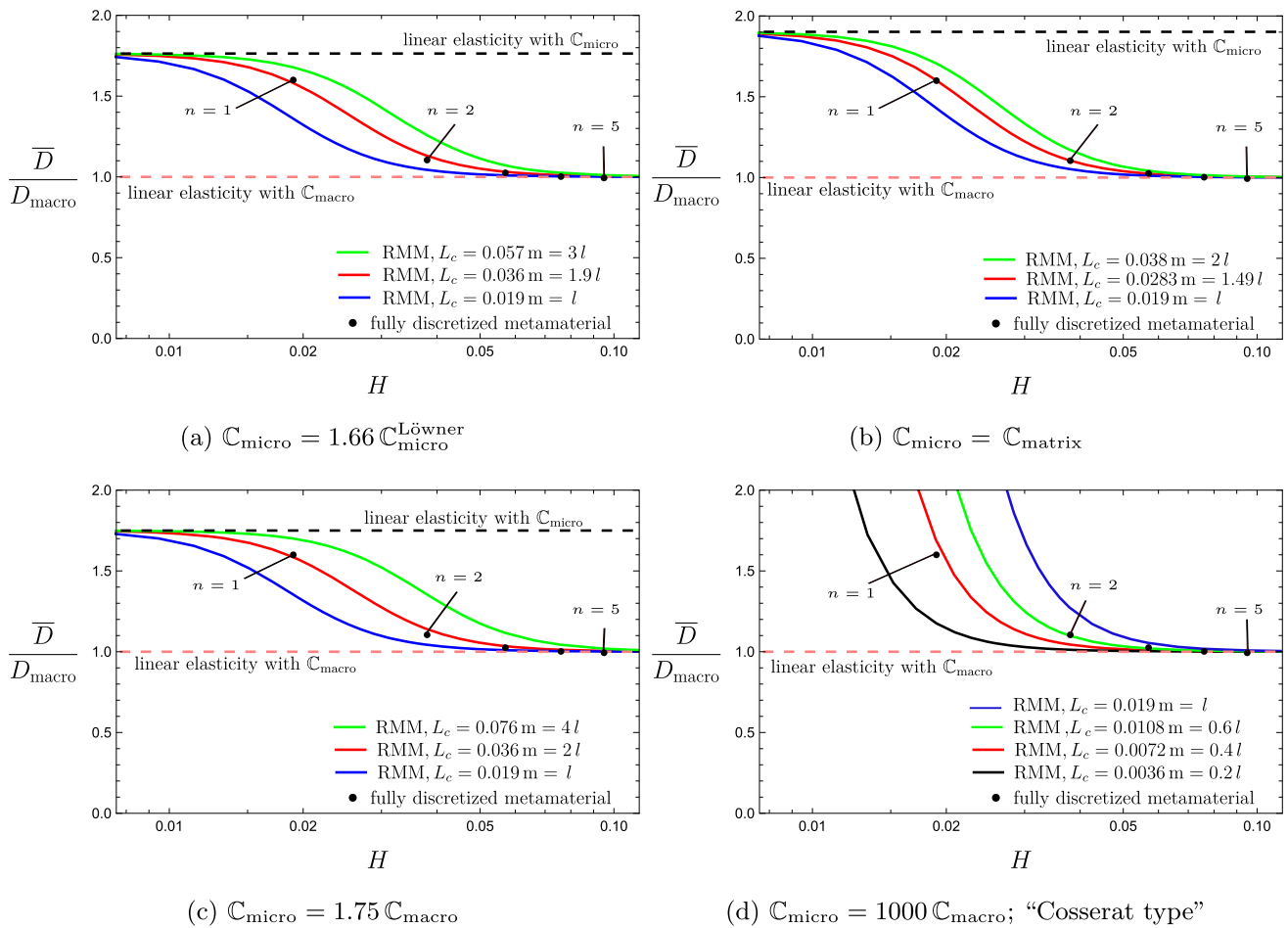
(a) $\mathbb{C}_{\mathrm{micro}} = 1.66\,\mathbb{C}_{\mathrm{micro}}^{\mathrm{L\ddot{o}wner}}$

(b) $\mathbb{C}_{\mathrm{micro}} = \mathbb{C}_{\mathrm{matrix}}$

(c) $\mathbb{C}_{\mathrm{micro}} = 1.75\,\mathbb{C}_{\mathrm{macro}}$

(d) $\mathbb{C}_{\mathrm{micro}} = 1000\,\mathbb{C}_{\mathrm{macro}}$; "Cosserat type"

Fig. 17 The normalized bending stiffness varying the beam size $H \times L = n\,l \times 12\,n\,l$ obtained by the fully discretized metamaterial and the relaxed micromorphic model. We analyze here different choices for $\mathbb{C}_{\mathrm{micro}}$ with varying L_c and fixing $\mu = \mu_{\mathrm{macro}}$. Assuming $\mathbb{C}_{\mathrm{micro}} = 10{,}000\,\mathbb{C}_{\mathrm{macro}}$ yields the same results as in (d)

6.1 Simple shearing

The boundary conditions are derived from the solution of an infinite stripe under simple shear in [85]

$$\boldsymbol{u} = \overline{\boldsymbol{u}} = \begin{pmatrix} ay \\ 0 \end{pmatrix} \qquad \text{on} \qquad \partial\mathcal{B}, \tag{40}$$

which leads to the following strain and stress tensors for the homogeneous macro-elasticity case

$$\overline{\boldsymbol{\varepsilon}} = \begin{pmatrix} 0 & a/2 \\ a/2 & 0 \end{pmatrix}, \qquad \overline{\boldsymbol{\sigma}} = \begin{pmatrix} 0 & a\,\mu_{\mathrm{macro}}^* \\ a\,\mu_{\mathrm{macro}}^* & 0 \end{pmatrix}. \tag{41}$$

The boundary value problems for the relaxed micromorphic model and the reference full detailed metamaterial are depicted in Fig. 19. Dirichlet boundary condition for the displacement field and the consistent coupling condition must be satisfied over the entire boundary.

The size-effect is analyzed through the relative shear force $\frac{T}{T_{\mathrm{macro}}}$, which is shown in Fig. 20. The macro-scale shear force is given by $T_{\mathrm{macro}} = a\,\mu_{\mathrm{macro}}^*\,L$. The shear response of the assumed metamaterial is less influenced by its size compared to its response to bending. We notice that the choices $\mathbb{C}_{\mathrm{micro}} = 1.66\,\mathbb{C}_{\mathrm{micro}}^{L\ddot{o}wner}$ and $\mathbb{C}_{\mathrm{micro}} = 1.75\,\mathbb{C}_{\mathrm{macro}}$ deliver close results for the bending in Fig. 17 but different results for the simple shear in Fig. 20 which can be explained by their different anisotropy properties.

6.2 Cantilever under traction load

In this setup, the right edge of the metamaterial is fixed in both directions while a constant traction of $t_y = \bar{t}$ is applied in the y-direction on the left side. The boundary value problems for both the fully discretized metamaterial and the relaxed micromorphic model are depicted in Fig. 21. The micro elasticity can be recovered for large values of L_c when a consistent coupling condition is applied to the entire boundary. How-
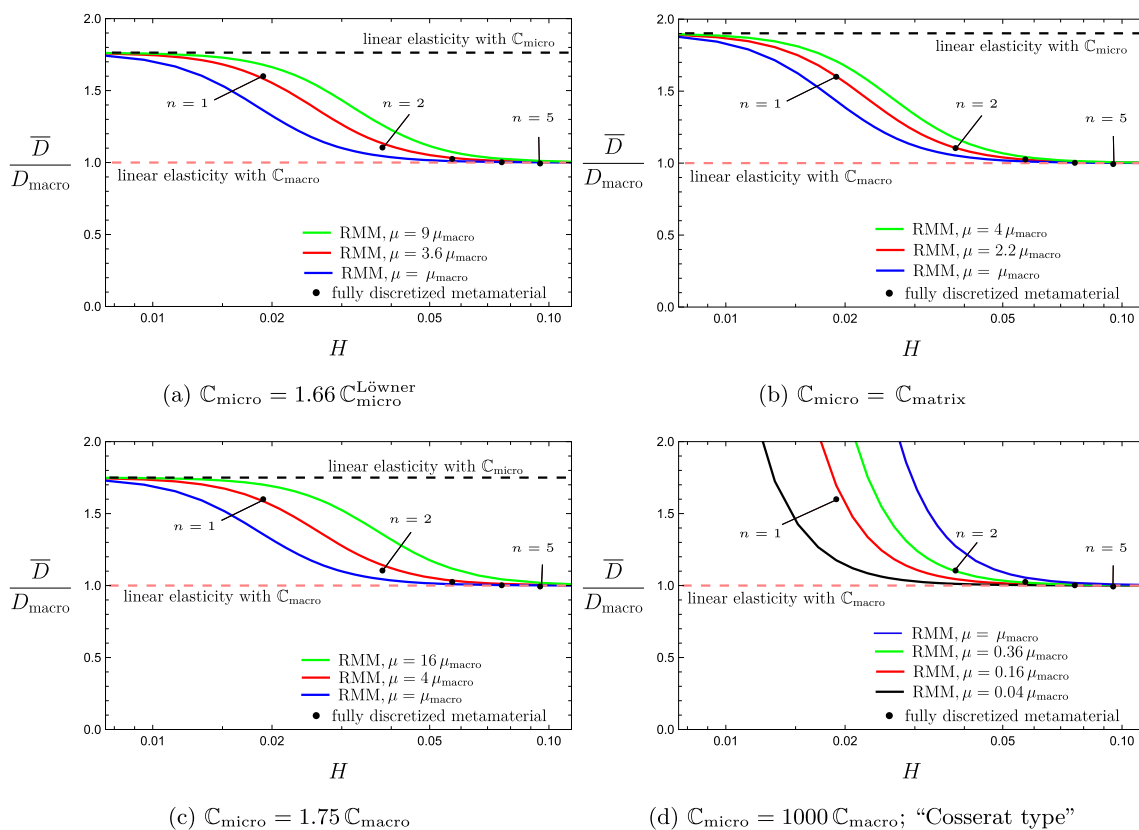
Fig. 18 The normalized bending stiffness varying the beam size $H \times L = n\,l \times 12\,n\,l$ obtained by the fully discretized metamaterial and the relaxed micromorphic model. We analyze here different choices for $\mathbb{C}_{\mathrm{micro}}$ with varying μ and fixing $L_{\mathrm{c}} = l$. The results are equivalent for both loading cases. The relaxed micromorphic model shows bounded stiffness given by $\mathbb{C}_{\mathrm{micro}}$ in contrast to the Cosserat model
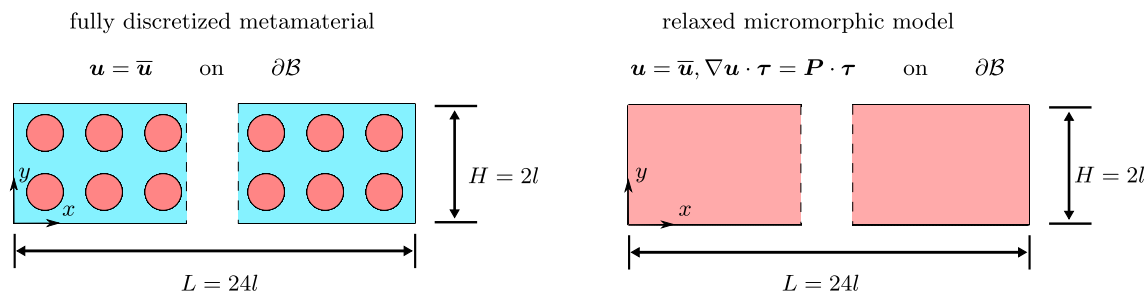

Fig. 19 The geometry of the boundary value problem (shear) shown for $n = 2$ for the fully discretized metamaterial and the homogeneous relaxed micrmorphic continuum

ever, for small values of L_{c}, a boundary layer is created at the upper and lower edges, requiring a fine mesh. This issue can be resolved by partially applying the consistent boundary condition, $(\nabla \boldsymbol{u} \cdot \boldsymbol{\tau})_y = (\boldsymbol{P} \cdot \boldsymbol{\tau})_y$.

The equivalent beam model of the assumed cantilever, with the deformed shape illustrated for $n = 2$, is displayed in Fig. 22. The cantilever is subjected to a constant shear force $F_y = \bar{t}\,H$ and a linear moment that is zero on the left end and maximum on the right end $M = F_y\,x$.

The size-effect is analyzed by determining the inverse of the relative maximum displacement, expressed as $\frac{w_{\mathrm{macro}}(0)}{w(0)}$.

This calculation is illustrated in Fig. 23. The macro-scale displacement is calculated using the formula $w_{\mathrm{macro}}(0) = \frac{4(1-\nu_{\mathrm{macro}}^2)F_y L^3}{E_{\mathrm{macro}} H^3}$. The results of both the fully discretized metamaterial and the relaxed micromorphic model show good agreement, as the dominant size-effect is bending. However, if consistent boundary conditions are not applied across the entire boundary, agreement is not achieved.
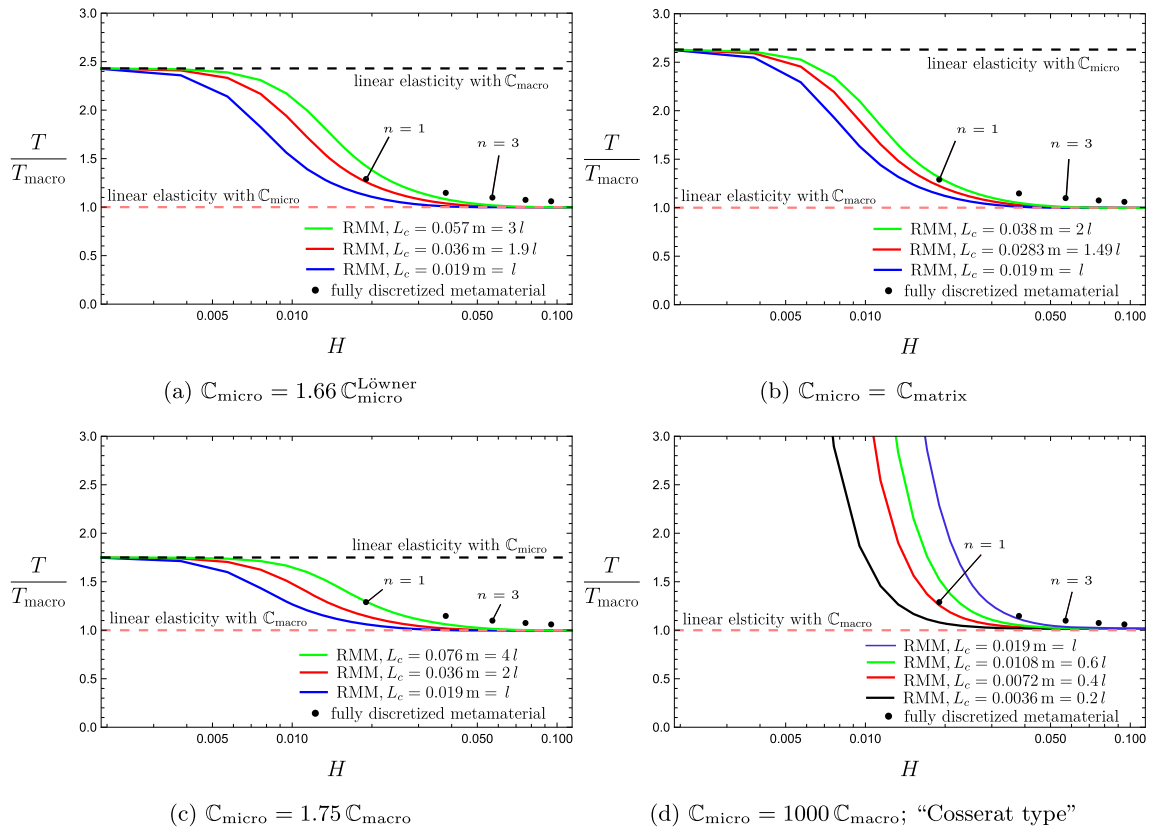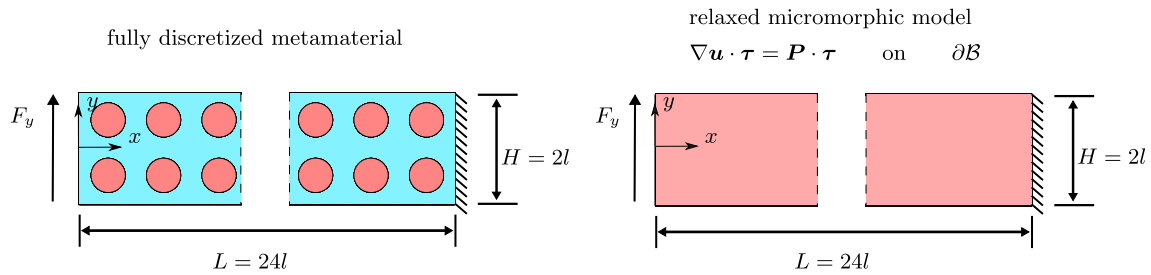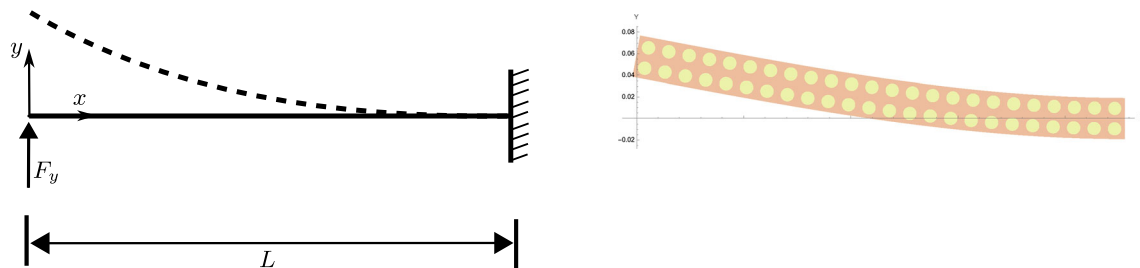
(a) $\mathbb{C}_{\mathrm{micro}} = 1.66\,\mathbb{C}_{\mathrm{micro}}^{\mathrm{L\ddot{o}wner}}$

(b) $\mathbb{C}_{\mathrm{micro}} = \mathbb{C}_{\mathrm{matrix}}$

(c) $\mathbb{C}_{\mathrm{micro}} = 1.75\,\mathbb{C}_{\mathrm{macro}}$

(d) $\mathbb{C}_{\mathrm{micro}} = 1000\,\mathbb{C}_{\mathrm{macro}};$ "Cosserat type"

Fig. 20 The relative shear force varying the specimen's size $H \times L$ for different choices of $\mathbb{C}_{\mathrm{micro}}$

Fig. 21 The geometry of the boundary value problem shown for $n = 2$ for the fully discretized metamaterial and the homogeneous relaxed micrmorphic continuum

Fig. 22 The beam model of the cantilever and the deformed shape for $H \times L = 2\,l \times 24\,l$

(a) $\mathbb{C}_{\mathrm{micro}} = 1.66\,\mathbb{C}_{\mathrm{micro}}^{\mathrm{L\ddot{o}wner}}$

(b) $\mathbb{C}_{\mathrm{micro}} = \mathbb{C}_{\mathrm{matrix}}$

(c) $\mathbb{C}_{\mathrm{micro}} = 1.75\,\mathbb{C}_{\mathrm{macro}}$

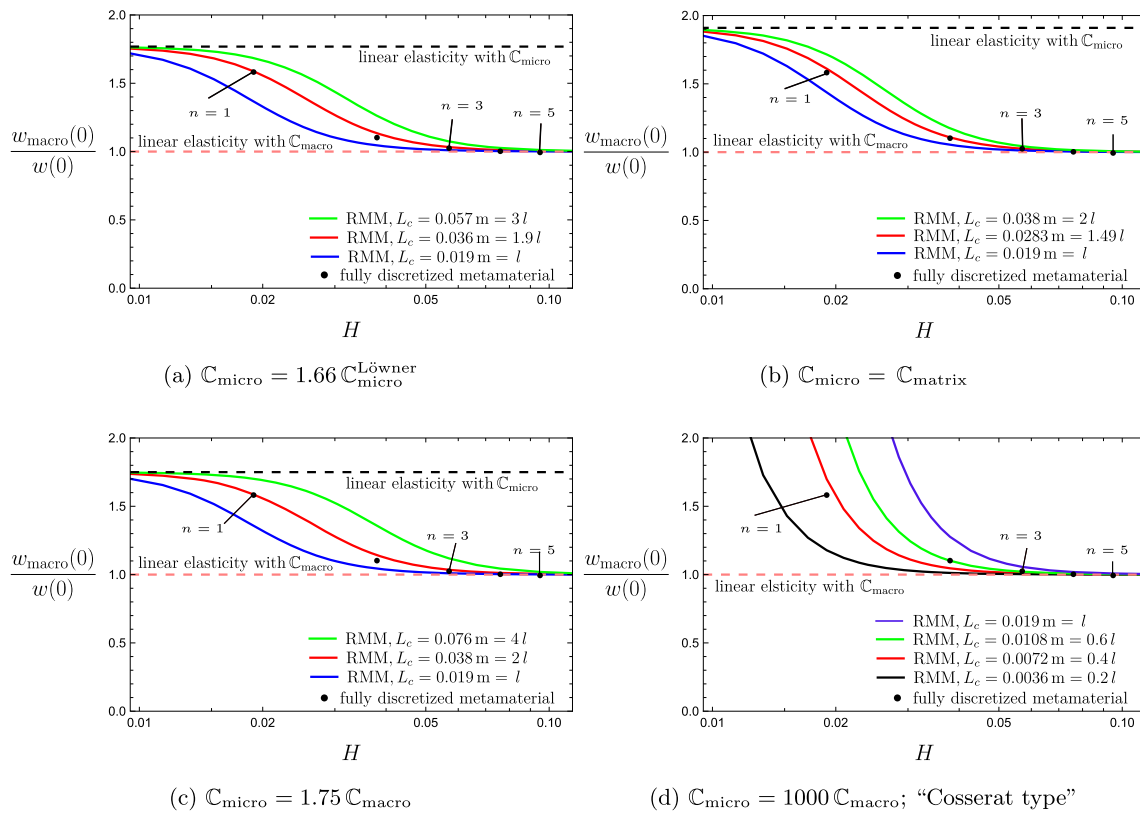(d) $\mathbb{C}_{\mathrm{micro}} = 1000\,\mathbb{C}_{\mathrm{macro}}$; "Cosserat type"

Fig. 23 The inverse of the relative deflection at the free end of the cantilever ($x = 0$) for varying the specimen's size $H \times L$ for different choices of $\mathbb{C}_{\mathrm{micro}}$

7 Conclusions

We introduced the relaxed micromorphic model with a brief description of the suitable tangential-conforming finite element formulation. We studied the size-effect phenomena of fully resolved beams under bending. We have shown that applying a rotation (via a given displacement) or moment (applied traction) on the fully discretized metamaterial leads to similar results which we should get as well when we use the relaxed micromorphic model. We defined the macro elasticity tensor $\mathbb{C}_{\mathrm{macro}}$ by means of the standard periodic homogenization corresponding to large specimens. The micro elasticity tensor is connected to the stiffest possible response of the assumed metamaterial. We introduced an approach to defining $\mathbb{C}_{\mathrm{micro}}$ which is based on the least upper bound of the apparent stiffness of the microstructure measured in the energy norm following the Löwner matrix supremum problem where different variants of unit cells are considered under the affine Dirichlet boundary conditions. However, the flexural deformation mode is not captured by affine Dirichlet boundary conditions and the resulting elasticity tensor is much softer than the bent fully resolved metamaterial beams. Therefore, we scaled up the resulting elasticity tensor keeping its anisotropic cubic sym-

metry. Another procedure is tested to identify the micro elasticity tensor by non-affine boundary conditions (bending) on the unit cell or cluster of unit cells with the possible largest flexural rigidity. The boundary conditions were investigated for both loading cases (rotation or moment) for the symmetric and non-symmetric force stress. The consistent coupling boundary condition permits the model to work on the whole intended range bounded by linear elasticity with micro and macro elasticity tensors from above and below, respectively. We scaled the curvature measurement, which is isotropic in 2D, to account for the beam's size where a final fitting is conducted to decide the values of characteristic length and the shear modulus associated with the Curl of the micro-distortion field. The relaxed micromorphic model delivers successfully the size-effects in a consistent manner for both loading cases. Finally, the relaxed micromorphic model was tested for two loading scenarios apart from pure bending with the consistent boundary condition applied on the entire boundary, highlighting its importance. Good agreement was obtained, however, the unique identification of the micro-elasticity tensor remains an open topic for future improvement. We established that the micro-elasticity tensor $\mathbb{C}_{\mathrm{micro}}$ must be stiffer than the apparent stiffness under the

affine Dirichlet boundary conditions, but not stiffer than the homogeneous matrix.

References

1. Abali BE (2019) Revealing the physical insight of a length-scale parameter in metamaterials by exploiting the variational formulation. Contin Mech Thermodyn 31:885–894

2. Abali BE, Barchiesi E (2021) Additive manufacturing introduced substructure and computational determination of metamaterials parameters by means of the asymptotic homogenization. Contin Mech Thermodyn 33:993–1009

3. Abali BE, Yang H, Papadopoulos P (2019) A computational approach for determination of parameters in generalized mechanics. In: Altenbach H, Müller WH, Abali BE (eds) Higher gradient materials and related generalized continua. Springer International Publishing, Cham, pp 1–18

4. Abali BE, Vazic B, Newell P (2022) Influence of microstructure on size effect for metamaterials applied in composite structures. Mech Res Commun 122:103877

5. Aifantis EC (2011) On the gradient approach—relation to Eringen's nonlocal theory. Int J Eng Sci 49(12):1367–1377

6. Aivaliotis A, Tallarico D, Agostino MV, Daouadji A, Neff P, Madeo A (2020) Frequency- and angle-dependent scattering of a finite-sized meta-structure via the relaxed micromorphic model. Arch Appl Mech 90:1073–1096

7. Al-Basyouni KS, Tounsi A, Mahmoud SR (2015) Size dependent bending and vibration analysis of functionally graded micro beams based on modified couple stress theory and neutral surface position. Compos Struct 125:621–630

8. Alavi SE, Ganghoffer J-F, Reda H, Sadighi M (2021) Construction of micromorphic continua by homogenization based on variational principles. J Mech Phys Solids 153:104278

9. Alavi SE, Ganghoffer J-F, Sadighi M (2022) Chiral Cosserat homogenized constitutive models of architected media based on micromorphic homogenization. Math Mech Solids 27(10):2287–2313

10. Alavi SE, Ganghoffer JF, Sadighi M, Nasimsobhan M, Akbarzadeh AH (2022) Continualization method of lattice materials and analysis of size effects revisited based on Cosserat models. Int J Solids Struct 254–255:111894

11. Altan BS, Aifantis EC (1997) On some aspects in the special theory of gradient elasticity. J Mech Behav Mater 8(3):231–282

12. Askes H, Aifantis EC (2011) Gradient elasticity in statics and dynamics: an overview of formulations, length scale identification procedures, finite element implementations and new results. Int J Solids Struct 48(13):1962–1990

13. Askes H, Metrikine AV, Pichugin AV, Bennett T (2008) Four simplified gradient elasticity models for the simulation of dispersive wave propagation. Philos Mag 88(28–29):3415–3443

14. Auffray N, Bouchet R, Bréchet Y (2010) Strain gradient elastic homogenization of bidimensional cellular media. Int J Solids Struct 47(13):1698–1710

15. Bacigalupo A, Gambarotta L (2010) Second-order computational homogenization of heterogeneous materials with periodic microstructure. J Appl Math Mech 90(10–11):796–811

16. Bacigalupo A, Paggi M, Dal Corso F, Bigoni D (2018) Identification of higher-order continua equivalent to a Cauchy elastic composite. Mech Res Commun 93:11–22. Mechanics from the 20th to the 21st Century: The Legacy of Gérard A. Maugin

17. Barbagallo G, Madeo A, d'Agostino MV, Abreu R, Ghiba I-D, Neff P (2017) Transparent anisotropy for the relaxed micromorphic model: macroscopic consistency conditions and long wave length asymptotics. Int J Solids Struct 120:7–30

18. Barbagallo G, Tallarico D, d'Agostino MV, Aivaliotis A, Neff P, Madeo A (2019) Relaxed micromorphic model of transient wave propagation in anisotropic band-gap metastructures. Int J Solids Struct 162:148–163

19. Berkache K, Deogekar S, Goda I, Picu RC, Ganghoffer J-F (2017) Construction of second gradient continuum models for random fibrous networks and analysis of size effects. Compos Struct 181:347–357

20. Biswas R, Poh LH (2017) A micromorphic computational homogenization framework for heterogeneous materials. J Mech Phys Solids 102:187–208

21. Blesgen T, Neff P (2022) Simple shear in nonlinear cosserat micropolar elasticity: existence of minimizers, numerical simulations, and occurrence of microstructure. Math Mech Solids 10812865221122191

22. Boutin C (1996) Microstructural effects in elastic composites. Int J Solids Struct 33(7):1023–1053

23. Carcaterra A, dell'Isola F, Esposito R, Pulvirenti M (2015) Macroscopic description of microscopically strongly inhomogenous systems: a mathematical basis for the synthesis of higher gradients metamaterials. Arch Ration Mech Anal 218:1239–1262

24. Cosserat E, Cosserat F (1909) Thèorie des corps dèformable. Librairie Scientifique A. Hermann et Fils, engl. translation by D. H. Delphenich, pdf available at http://www.mathematik.tu-darmstadt.de/fbereiche/analysis/pde/staff/neff/patrizio/Cosserat.html reprint 2009 by Hermann Librairie Scientifique, ISBN 978 27056 6920 1, Paris

25. d'Agostino MV, Barbagallo G, Ghiba I-D, Eidel B, Neff P, Madeo A (2020) Effective description of anisotropic wave dispersion in mechanical band-gap metamaterials via the relaxed micromorphic model. J Elast 139:299–329

26. d'Agostino MV, Rizzi G, Khan H, Lewintan P, Madeo A, Neff P (2022) The consistent coupling boundary condition for the classical micromorphic model: existence, uniqueness and interpretation of the parameters. Contin Mech Thermodyn. https://doi.org/10.1007/s00161-022-01126-3

27. Del Vescovo D, Giorgio I (2014) Dynamic problems for metamaterials: review of existing models and ideas for further research. Int J Eng Sci 80:153–172

28. Demore F, Rizzi G, Collet M, Neff P, Madeo A (2022) Unfolding engineering metamaterials design: relaxed micromorphic model-

ing of large-scale acoustic meta-structures. J Mech Phys Solids 168:104995

29. El Dhaba AR (2020) Reduced micromorphic model in orthogonal curvilinear coordinates and its application to a metamaterial hemisphere. Sci Rep 10:2846

30. Eremeyev VA, Cazzani A, dell'Isola F (2021) On nonlinear dilatational strain gradient elasticity. Contin Mech Thermodyn 33:1429–1463

31. Eringen AC (1968) Mechanics of micromorphic continua. In: Mechanics of generalized continua. Springer, Berlin, Heidelberg, pp 18–35

32. Eringen AC, Suhubi ES (1964) Nonlinear theory of simple micro-elastic solids-I. Int J Eng Sci 2(2):189–203

33. Fischer P, Klassen M, Mergheim J, Steinmann P, Müller R (2011) Isogeometric analysis of 2D gradient elasticity. Comput Mech 47:1432–0924

34. Fischer SCL, Hillen L, Eberl C (2020) Mechanical metamaterials on the way from laboratory scale to industrial applications: challenges for characterization and scalability. Materials 13(16):3605

35. Forest S (2002) Homogenization methods and mechanics of generalized continua—part 2. Theor Appl Mech 28–29:113–144

36. Forest S (2016) Nonlinear regularization operators as derived from the micromorphic approach to gradient elasticity, viscoplasticity and damage. Proc R Soc 472(2188):20150755

37. Forest S, Sab K (1998) Cosserat overall modeling of heterogeneous materials. Mech Res Commun 25(4):449–454

38. Forest S, Trinh DK (2011) Generalized continua and non-homogeneous boundary conditions in homogenisation methods. J Appl Math Mech 91(2):90–109

39. Ganghoffer J-F, Reda H (2021) A variational approach of homogenization of heterogeneous materials towards second gradient continua. Mech Mater 158:103743, ISSN 0167-6636. https://doi.org/10.1016/j.mechmat.2021.103743. https://www.sciencedirect.com/science/article/pii/S0167663621000028

40. Ghiba I-D, Neff P, Madeo A, Placidi L, Rosi G (2015) The relaxed linear micromorphic continuum: existence, uniqueness and continuous dependence in dynamics. Math Mech Solids 20(10):1171–1197

41. Ghiba I-D, Rizzi G, Madeo A, Neff P (2022) Cosserat micropolar elasticity: classical Eringen vs. dislocation form. https://arxiv.org/abs/2206.02473. To appear in Journal of Mechanics of Materials and Structures

42. Glaesener RN, Bastek J-H, Gonon F, Kannan V, Telgen B, Spöttling B, Steiner S, Kochmann DM (2021) Viscoelastic truss metamaterials as time-dependent generalized continua. J Mech Phys Solids 156:104569

43. Goda I, Ganghoffer J-F (2016) Construction of first and second order grade anisotropic continuum media for 3D porous and textile composite structures. Compos Struct 141:292–327

44. Golaszewski M, Grygoruk R, Giorgio I, Laudato M, Cosmo FD (2019) Metamaterials with relative displacements in their microstructure: technological challenges in 3d printing, experiments and numerical predictions. Contin Mech Thermodyn 31:1015–1034

45. Hosseini SB, Niiranen J (2022) 3D strain gradient elasticity: variational formulations, isogeometric analysis and model peculiarities. Comput Methods Appl Mech Eng 389:114324

46. Hütter G (2017) Homogenization of a Cauchy continuum towards a micromorphic continuum. J Mech Phys Solids 99:394–408

47. Hütter G (2019) On the micro-macro relation for the microdeformation in the homogenization towards micromorphic and micropolar continua. J Mech Phys Solids 127:62–79

48. Hütter G (2022) Interpretation of micromorphic constitutive relations for porous materials at the microscale via harmonic decomposition. J Mech Phys Solids 171:105135

49. Ju X, Mahnken R, Liang L, Xu Y (2021) Goal-oriented mesh adaptivity for inverse problems in linear micromorphic elasticity. Comput Struct 257:106671

50. Khakalo S, Niiranen J (2019) Lattice structures as thermoelastic strain gradient metamaterials: evidence from full-field simulations and applications to functionally step-wise-graded beams. Compos Part B Eng 177:107224

51. Khakalo S, Niiranen J (2020) Anisotropic strain gradient thermoelasticity for cellular structures: plate models, homogenization and isogeometric analysis. J Mech Phys Solids 134:103728

52. Khakalo S, Balobanov V, Niiranen J (2018) Modelling size-dependent bending, buckling and vibrations of 2D triangular lattices by strain gradient elasticity models: applications to sandwich beams and auxetics. Int J Eng Sci 127:33–52

53. Khan H, Ghiba I-D, Madeo A, Neff P (2022) Existence and uniqueness of Rayleigh waves in isotropic elastic Cosserat materials and algorithmic aspects. Wave Motion 110:102898

54. Kirby RC, Logg A, Rognes ME, Terrel AR (2012) Common and unusual finite elements. In: Automated solution of differential equations by the finite element method: the FEniCS book. Springer Berlin Heidelberg, Berlin, Heidelberg, pp 95–119

55. Knees D, Owczarek S, Neff P (2022) A local regularity result for the relaxed micromorphic model based on inner variations. To appear in Journal of Mathematical Analysis and Applications. https://doi.org/10.48550/ARXIV.2208.04821

56. Korelc J (2009) Automation of primal and sensitivity analysis of transient coupled problems. Comput Mech 44(5):631–649

57. Korelc J, Wriggers P (2016) Automation of finite element methods. Springer, Berlin

58. Kouznetsova V, Geers MGD, Brekelmans WAM (2002) Multiscale constitutive modelling of heterogeneous materials with a gradient-enhanced computational homogenization scheme. Int J Numer Methods Eng 54:1235–1260

59. Kouznetsova V, Geers MGD, Brekelmans WAM (2004) Multiscale second-order computational homogenization of multi-phase materials: a nested finite element solution strategy. Comput Methods Appl Mech Eng 193:5525–5550

60. Lahbazi A, Goda I, Ganghoffer J-F (2022) Size-independent strain gradient effective models based on homogenization methods: applications to 3D composite materials, pantograph and thin walled lattices. Compos Struct 284:115065

61. Lakes RS (2022) Cosserat shape effects in the bending of foams. Mech Adv Mater Struct. https://doi.org/10.1080/15376494.2022.2086328

62. Lee J-H, Singer JP, Thomas EL (2012) Micro-/nanostructured mechanical metamaterials. Adv Mater 24(36):4782–4810

63. Leismann T, Mahnken R (2015) Comparison of hyperelastic micromorphic, micropolar and microstrain continua. Int J Non-Linear Mech 77:115–127

64. Li A, Wang Q, Song M, Chen J, Su W, Zhou S, Wang L (2022) On strain gradient theory and its application in bending of beam. Coatings 12(9):1304

65. Li J, Zhang X-B (2013) A numerical approach for the establishment of strain gradient constitutive relations in periodic heterogeneous materials. Eur J Mech A/Solids 41:70–85

66. Liebold C, Müller WH (2016) Comparison of gradient elasticity models for the bending of micromaterials. Comput Mater Sci 116:52–61

67. Madeo A, Neff P, Ghiba I-D, Placidi L, Rosi G (2015) Band gaps in the relaxed linear micromorphic continuum. Z Angew Math Mech 95(9):880–887

68. Madeo A, Neff P, d'Agostino MV, Barbagallo G (2016) Complete band gaps including non-local effects occur only in the relaxed micromorphic model. Comptes Rendus Mécanique 344(11–12):784–796

69. Madeo A, Neff P, Ghiba I-D, Rosi G (2016) Reflection and transmission of elastic waves in non-local band-gap metamaterials: a comprehensive study via the relaxed micromorphic model. J Mech Phys Solids 95:441–479

70. Madeo A, Neff P, Barbagallo G, d'Agostino MV, Ghiba I-D (2017) A review on wave propagation modeling in band-gap metamaterials via enriched continuum models. In: Mathematical modelling in solid mechanics, volume 69 of advanced structured materials. Springer, Singapore, pp 89–105

71. Mindlin RD (1964) Micro-structure in linear elasticity. Arch Ration Mech Anal 16:51–78

72. Mindlin RD, Eshel NN (1968) On first strain-gradient theories in linear elasticity. Int J Solids Struct 4(1):109–124

73. Monchiet V, Auffray N, Yvonne J (2020) Strain-gradient homogenization: a bridge between the asymptotic expansion and quadratic boundary condition methods. Mech Mater 143:103309

74. Nédélec JC (1980) Mixed finite elements in $\mathbb{R}^3$. Numer Math 35(3):315–341

75. Nédélec JC (1986) A new family of mixed finite elements in $\mathbb{R}^3$. Numer Math 50:57–81

76. Neff P (2006) The Cosserat couple modulus for continuous solids is zero viz the linearized Cauchy-stress tensor is symmetric. Z Angew Math Mech 86(11):892–912

77. Neff P, Forest S (2007) A geometrically exact micromorphic model for elastic metallic foams accounting for affine microstructure. Modelling, existence of minimizers, identification of moduli and computational results. J Elast 87(2):239–276

78. Neff P, Jeong J, Münch I, Ramézani H (2010) Linear Cosserat elasticity, conformal curvature and bounded stiffness. In: Mechanics of generalized continua: one hundred years after the cosserats. Springer, New York, pp 55–63

79. Neff P, Ghiba I-D, Madeo A, Placidi L, Rosi G (2014) A unifying perspective: the relaxed linear micromorphic continuum. Contin Mech Thermodyn 26(5):639–681

80. Neff P, Ghiba ID, Lazar M, Madeo A (2015) The relaxed linear micromorphic continuum: well-posedness of the static problem and relations to the gauge theory of dislocations. Q J Mech Appl Math 68(1):53–84

81. Neff P, Eidel B, d'Agostino MV, Madeo A (2020) Identification of scale-independent material parameters in the relaxed micromorphic model through model-adapted first order homogenization. J Elast 139:269–298

82. Owczarek S, Ghiba I-D, d'Agostino MV, Neff P (2019) Nonstandard micro-inertia terms in the relaxed micromorphic model: well-posedness for dynamics. Math Mech Solids 24(10):3200–3215

83. Placidi L, Barchiesi E, Battista A (2017) An inverse method to get further analytical solutions for a class of metamaterials aimed to validate numerical integrations. In: dell'Isola F, Sofonea M, Steigmann D (eds) Mathematical modelling in solid mechanics. Springer, Singapore, pp 193–210

84. Reda H, Alavi SE, Nasimsobhan M, Ganghoffer J-F (2021) Homogenization towards chiral Cosserat continua and applications to enhanced Timoshenko beam theories. Mech Mater 155:103728

85. Rizzi G, Hütter G, Madeo A, Neff P (2021) Analytical solutions of the simple shear problem for micromorphic models and other generalized continua. Arch Appl Mech 91:2237–2254

86. Rizzi G, Hütter G, Madeo A, Neff P (2021) Analytical solutions of the cylindrical bending problem for the relaxed micromorphic continuum and other generalized continua. Contin Mech Thermodyn 33:1505–1539

87. Rizzi G, Khan H, Ghiba I-D, Madeo A, Neff P (2021) Analytical solution of the uniaxial extension problem for the relaxed micromorphic continuum and other generalized continua (including full

derivations). Arch Appl Mech. https://doi.org/10.1007/s00419-021-02064-3

88. Rizzi G, d'Agostino MV, Neff P, Madeo A (2022) Boundary and interface conditions in the relaxed micromorphic model: exploring finite-size metastructures for elastic wave control. Math Mech Solids 27(6):1053–1068

89. Rizzi G, Hütter G, Khan H, Ghiba I-D, Madeo A, Neff P (2022) Analytical solution of the cylindrical torsion problem for the relaxed micromorphic continuum and other generalized continua (including full derivations). Math Mech Solids 27(3):507–553

90. Rizzi G, Neff P, Madeo A (2022) Metamaterial for inner protection and outer tuning through a relaxed micromorphic approach. Philos Trans R Soc A Math Phys Eng Sci 380(2231):20210400

91. Rizzi G, Tallarico D, Neff P, Madeo A (2022) Towards the conception of complex engineering meta-structures: relaxed-micromorphic modelling of low-frequency mechanical diodes/high-frequency screens. Wave Motion 113:102920

92. Rognes ME, Kirby RC, Logg A (2009) Efficient assembly of $H(\mathrm{div})$ and $H(\mathrm{curl})$ conforming finite elements. SIAM J Sci Comput 31(9):4130–4151

93. Rokoš O, Ameen MM, Peerlings RHJ, Geers MGD (2019) Micromorphic computational homogenization for mechanical metamaterials with patterning fluctuation fields. J Mech Phys Solids 123:119–137

94. Rokoš O, Ameen MM, Peerlings RHJ, Geers MGD (2020) Extended micromorphic computational homogenization for mechanical metamaterials exhibiting multiple geometric pattern transformations. Extreme Mech Lett 37:100708

95. Rokoš O, Zeman J, Doškář M, Krysl P (2020) Reduced integration schemes in micromorphic computational homogenization of elastomeric mechanical metamaterials. Adv Model Simul Eng Sci 7:1–17

96. Rueger Z, Ha CS, Lakes RS (2019) Cosserat elastic lattices. Meccanica 54:1983–1999

97. Sarhil M, Scheunemann L, Neff P, Schröder J (2021) On a tangential-conforming finite element formulation for the relaxed micromorphic model in 2D. Proc Appl Math Mech 21(1):e202100187

98. Sarhil M, Scheunemann L, Schröder J, Neff P (2023) Modeling the size-effect of metamaterial beams under bending via the relaxed micromorphic continuum. Proc Appl Math Mech 22(1):e202200033

99. Schmidt F, Krüger M, Keip M-A, Hesch C (2022) Computational homogenization of higher-order continua. Int J Numer Methods Eng 123(11):2499–2529

100. Schröder J, Sarhil M, Scheunemann L, Neff P (2022) Lagrange and $H(curl, \mathcal{B})$ based Finite Element formulations for the relaxed micromorphic model. Comput Mech 70(6):1309–1333. https://doi.org/10.1007/s00466-022-02198-3

101. Shekarchizadeh N, Abali BE, Barchiesi E, Bersani AM (2021) Inverse analysis of metamaterials and parameter determination by means of an automatized optimization problem. Z Angew Math Mech 101(8):e202000277

102. Shekarchizadeh N, Abali BE, Bersani AM (2022) A benchmark strain gradient elasticity solution in two-dimensions for verifying computational approaches by means of the finite element method. Math Mech Solids 27(10):2218–2238

103. Shi F, Fantuzzi N, Trovalusci P, Li Y, Wei Z (2022) Stress field evaluation in orthotropic microstructured composites with holes as Cosserat continuum. Materials 15(18):6196

104. Skrzat A, Eremeyev VA (2020) On the effective properties of foams in the framework of the couple stress theory. Contin Mech Thermodyn 32:1779–1801

105. Sky A, Neunteufel M, Münch I, Schöberl J, Neff P (2021) A hybrid $H^1 \times H(\mathrm{curl})$ finite element formulation for a relaxed

micromorphic continuum model of antiplane shear. Comput Mech 68:1–24

106. Sky A, Neunteufel M, Münch I, Schöberl J, Neff P (2022) Primal and mixed finite element formulations for the relaxed micromorphic model. Comput Methods Appl Mech Eng 399:115298

107. Sky A, Münch I, Rizzi G, Neff P (2023) Higher order Bernstein-Bézier and Nédélec finite elements for the relaxed micromorphic model. https://doi.org/10.48550/ARXIV.2301.01491

108. Sridhar A, Kouznetsova VG, Geers MGD (2016) Homogenization of locally resonant acoustic metamaterials towards an emergent enriched continuum. Comput Mech 57:423–435

109. Sridhar A, Liu L, Kouznetsova VG, Geers MGD (2018) Homogenized enriched continuum analysis of acoustic metamaterials with negative stiffness and double negative effects. J Mech Phys Solids 119:104–117

110. Suhubl ES, Eringen AC (1964) Nonlinear theory of micro-elastic solids-II. Int J Eng Sci 2(4):389–404

111. Surjadi JU, Gao L, Du H, Li X, Xiong X, Fang NX, Lu Y (2019) Mechanical metamaterials and their engineering applications. Adv Eng Mater 21(3):1800864

112. Tran T-H, Monchiet V, Bonnet G (2012) A micromechanics-based approach for the derivation of constitutive elastic coefficients of strain-gradient media. Int J Solids Struct 49(5):783–792

113. Trinh DK, Jänicke R, Auffray N, Diebels S, Forest S (2012) Evaluation of generalized continuum substitution models for heterogeneous materials. Int J Multiscale Comput Eng 10(6):527–549

114. Trovalusci P, Pau A (2014) Derivation of microstructured continua from lattice systems via principle of virtual works: the case of masonry-like materials as micropolar, second gradient and classical continua. Acta Mech 225:157–177. https://doi.org/10.1007/s00707-013-0936-9

115. Waseem A, Heuzé T, Stainier L, Geers MGD, Kouznetsova VG (2020) Enriched continuum for multi-scale transient diffusion coupled to mechanics. Adv Model Simul Eng Sci 7:1–32

116. Weeger O (2021) Numerical homogenization of second gradient, linear elastic constitutive models for cubic 3D beam-lattice metamaterials. Int J Solids Struct 224:111037

117. Yang H, Müller WH (2021) Size effects of mechanical metamaterials: a computational study based on a second-order asymptotic homogenization method. Arch Appl Mech 91:1037–1053

118. Yang H, Abali BE, Timofeev D, Müller WH (2020) Determination of metamaterial parameters by means of a homogenization approach based on asymptotic analysis. Contin Mech Thermodyn 32:1251–1270

119. Yang H, Timofeev D, Abali BE, Li B, Müller WH (2021) Verification of strain gradient elasticity computation by analytical solutions. Z Angew Math Mech 101(12):e202100023

120. Yang H, Abali BE, Müller WH, Barboura S, Li J (2022) Verification of asymptotic homogenization method developed for periodic architected materials in strain gradient continuum. Int J Solids Struct 238:111386

121. Yin S, Xiao Z, Deng Y, Zhang G, Liu J, Gu S (2021) Isogeometric analysis of size-dependent Bernoulli–Euler beam based on a reformulated strain gradient elasticity theory. Comput Struct 253:106577

122. Yu X, Zhou J, Liang H, Jiang Z, Wu L (2018) Mechanical metamaterials associated with stiffness, rigidity and compressibility: a brief review. Prog Mater Sci 94:114–173

123. Yvonnet J, Auffray N, Monchiet V (2020) Computational second-order homogenization of materials with effective anisotropic strain-gradient behavior. Int J Solids Struct 191–192:434–448

124. Zadpoor AA (2016) Mechanical meta-materials. Mater Horizons 3:371–381

125. Zhi J, Poh LH, Tay T-E, Tan VBC (2022) Direct FE2 modeling of heterogeneous materials with a micromorphic computational homogenization framework. Comput Methods Appl Mech Eng 393:114837

126. Zohdi TI, Wriggers P (2005) An introduction to computational micromechanics. Springer, Berlin